

วิธีการเคอร์คินไม่ต่อเนื่องแบบปรับตัวได้สำหรับสมการน้ำตื้นหนึ่งมิติ

นางสาวธิดา พงศ์สงวนสิน

วิทยานิพนธ์นี้เป็นส่วนหนึ่งของการศึกษาตามหลักสูตรปริญญาวิทยาศาสตรมหาบัณฑิต

สาขาวิชาคณิตศาสตร์ประยุกต์และวิทยาการคอมพิวเตอร์

ภาควิชาคณิตศาสตร์และวิทยาการคอมพิวเตอร์

คณะวิทยาศาสตร์ จุฬาลงกรณ์มหาวิทยาลัย

ปีการศึกษา 2554

ลิขสิทธิ์ของจุฬาลงกรณ์มหาวิทยาลัย

บทคัดย่อและแฟ้มข้อมูลฉบับเต็มของวิทยานิพนธ์ตั้งแต่ปีการศึกษา 2554 ที่ให้บริการในคลังปัญญาจุฬาฯ (CUIR)
เป็นแฟ้มข้อมูลของนิสิตเจ้าของวิทยานิพนธ์ที่ส่งผ่านทางบัณฑิตวิทยาลัย

The abstract and full text of theses from the academic year 2011 in Chulalongkorn University Intellectual Repository(CUIR)
are the thesis authors' files submitted through the Graduate School.

ADAPTIVE DISCONTINUOUS GALERKIN METHOD FOR ONE-DIMENSIONAL
SHALLOW WATER EQUATIONS

Miss Thida Pongsanguansin

A Thesis Submitted in Partial Fulfillment of the Requirements
for the Degree of Master of Science Program in Applied Mathematics
and Computational Science

Department of Mathematics and Computer Science

Faculty of Science

Chulalongkorn University

Academic Year 2011

Copyright of Chulalongkorn University

ธิดา พงศ์สงวนสิน : วิธีกาลเลอร์किन ไม่ต่อเนื่องแบบปรับตัวได้สำหรับสมการน้ำตื้นหนึ่งมิติ. (ADAPTIVE DISCONTINUOUS GALERKIN METHOD FOR ONE-DIMENSIONAL SHALLOW WATER EQUATIONS) อ.ที่ปรึกษาวิทยานิพนธ์หลัก : ดร. คำรณ เมฆฉาย, อ.ที่ปรึกษาวิทยานิพนธ์ร่วม : ผศ. ดร. มนตรี มาลีวงศ์, 64 หน้า.

ในวิทยานิพนธ์นี้ เรานำวิธีกาลเลอร์किन ไม่ต่อเนื่องมาใช้หาผลเฉลยโดยประมาณของสมการแอคเวชันและสมการน้ำตื้นหนึ่งมิติ และเพื่อเพิ่มประสิทธิภาพของวิธีนี้ เรานำหลักการปรับตัวได้สองแบบมาใช้ได้แก่ หลักการปรับตัวโดยดีกรีพหุนาม (p-adaptive) และหลักการปรับตัวขนาดของเซลล์ (h-adaptive) จุดประสงค์หลักเพื่อทำให้ผลเฉลยที่ได้จากการประมาณมีความแม่นยำมากขึ้นในขั้นตอนการหาปริพันธ์ในเวลา เซลล์ที่มีปัญหาซึ่งควรมีการปรับตัวสามารถตรวจจับได้ด้วยตัวบ่งชี้ความผิดพลาดสองชนิดคือ ค่าความผิดพลาดและค่าเกรเดียนต์ เราประยุกต์ใช้หลักการปรับตัวนี้เพื่อหาผลเฉลยของทั้งสมการแอคเวชันและสมการน้ำตื้นมาตรฐาน โดยสมการน้ำตื้นนั้นเราทำทั้งในกรณีที่ด้านท้ายน้ำเปียกและแห้ง และสามารถตรวจจับ shock ที่เคลื่อนที่ไปได้โดยหลักการปรับตัวขนาดของเซลล์ เมื่อใช้วิธี HLL ในการประมาณค่าของฟลักซ์ที่ขอบของเซลล์

ภาควิชา	คณิตศาสตร์ และ.....	ลายมือชื่อนิสิต.....
	วิทยาการคอมพิวเตอร์.....	
สาขาวิชา	คณิตศาสตร์ประยุกต์ และ.....	ลายมือชื่อ อ.ที่ปรึกษาวิทยานิพนธ์หลัก.....
	วิทยาการคณนา.....	ลายมือชื่อ อ.ที่ปรึกษาวิทยานิพนธ์ร่วม.....
ปีการศึกษา	2554.....	

5272342023 : MAJOR APPLIED MATHEMATICS AND COMPUTATIONAL SCIENCE

KEYWORDS : ADAPTIVE DISCONTINUOUS GALERKIN METHOD / SHALLOW WATER EQUATIONS

THIDA PONGSANGUANSIN : ADAPTIVE DISCONTINUOUS GALERKIN METHOD FOR ONE-DIMENSIONAL SHALLOW WATER EQUATIONS. THESIS ADVISOR : KHAMRON MEKCHAY, Ph.D. THESIS COADVISOR : ASSISTANT PROFESSOR MONTRI MALEEWONG, 64 pp.

The Discontinuous Galerkin (DG) method for solving the one-dimensional advection equation and shallow water equations are presented in this thesis. To improve the efficiency of this method, two types of adaptive technique are employed. These are the adaptive polynomial (p-adaptive) and the adaptive mesh (h-adaptive). The main purpose is to improve the accuracy of numerical solution during time integration process. Troubled cells needed to be refined are detected by two types of indicators, which are error and gradient indicators. The present schemes have been applied for solving the advection equation and the standard shallow water equations for both wet bed and dry bed. The moving shock can be detected correctly by the adaptive mesh criteria when the HLL flux approximation is employed at the interface of cell volume.

Department : Mathematics and..... Student's Signature

Computer Science.....

Field of Study : Applied Mathematics and..... Advisor's Signature

Computational Science..... Co-advisor's Signature

Academic Year : 2011.....

ACKNOWLEDGEMENTS

First of all, I am deeply indebted to my thesis advisor, Khamron Mekchay, Ph.D. and thesis co-advisor, Assisitant Professor Montri Maleewong, Ph.D. for their willingness to sacrifice to support, suggest and advice this thesis, and moreover, they always encourage me in this thesis work. I also would like to sincere thank the dissertation committee, Associate Professor Pornchai Satravaha, Ph.D., Assistant Professor Vimolrat Ngamaramvaranggul, Ph.D., Petarpa Boonserm, Ph.D. and Puntip Toghaw, Ph.D., for their insightful suggestion on my work. Sincere thank is also extended to all teachers who have taught me. Moreover, I would like to thank my friends for encourage me during this thesis work and thank the Science Achivement Scholarship Thailand (SAST) for the financial support since I was in undergraduate student.

Finally, I am very grateful to my family, for their love, encouragement and support. They are the most important persons in my life. Especially, I would like to express my deep gratitude to my parents for always taking care of me and giving me many useful advices. I feel very glad and pround to be their daughter.

CONTENTS

	page
ABSTRACT IN THAI	iv
ABSTRACT IN ENGLISH	v
ACKNOWLEDGEMENTS	vi
CONTENTS	vii
LIST OF TABLES	ix
LIST OF FIGURES	xi
CHAPTER	
I INTRODUCTION	1
II DERIVATION OF SHALLOW WATER EQUATIONS	4
2.1 Conservation Laws	4
2.2 Derivation of shallow water equations.....	5
2.3 Conservation of mass.....	6
2.4 Conservation of momentum.....	7
III NUMERICAL METHOD	11
3.1 The Discontinuous Galerkin (DG) scheme for the one-dimensional scalar conservation law	11
3.1.1 Convergence analysis of linear case	13
3.1.2 Numerical flux	14
3.1.3 Total Variation Diminishing Runge Kutta (TVD-RK)	14
3.1.4 The MUSCL slope limiter	16
3.2 Discontinuous Galerkin method for the one-dimensional shallow water equations	17
3.2.1 Numerical flux	19
3.2.2 The TVD-RK time discretization and slope limiter for the SWE ..	20
IV ADAPTIVE METHOD	21
4.1 Indicators	21
4.2 Adaptive polynomial for RKDG method (p-adaptive)	22

4.3 Adaptive mesh for RKDG method (h-adaptive)	24
V NUMERICAL RESULTS AND DISCUSSIONS	27
5.1 Advection Equation	27
5.1.1 RKDG method without adaptive criteria for advection equation .	28
5.1.2 Adaptive polynomial RKDG method for advection equation	32
5.1.3 Adaptive mesh RKDG method for advection equation	38
5.2 Shallow Water Equations	45
5.2.1 RKDG method without adaptive mesh criteria for shallow water equation	46
5.2.2 Adaptive mesh RKDG method for the shallow water equation ...	49
VI CONCLUSIONS	61
REFERENCES	62
VITA	64

LIST OF TABLES

TABLE	page
5.1	The RMS errors and rate of convergences when using the RKDG method for $N = 1, 2,$ and $3,$ and using $K = 20, 40, 80,$ and 160 29
5.2	The RMS errors for RKDG method using $N = 1, 2,$ and 3 and $K = 20, 40, 80,$ and 160 32
5.3	The RMS errors using error indicator with $K = 100$ cells and for some values of θ_1 and θ_2 34
5.4	The RMS errors when using the gradient indicator with $K = 100$ cells for some values of θ_1 and θ_2 37
5.5	The RMS error when using error indicator with $K=100, N=1$ for some values of θ_1 and θ_2 40
5.6	The RMS error when using error indicator with $K=100, N=2$ for some values of θ_1 and θ_2 41
5.7	The RMS error when using gradient indicator with $K=100, N=1$ for some values of θ_1 and θ_2 43
5.8	The RMS error when using gradient indicator with $K = 100$ cells, polynomial degree $N = 2$ for some values of θ_1 and θ_2 44
5.9	Some values of h_2, u_2 and V when a is given 46
5.10	The RMS errors using $N = 1$ and $N = 2$ with $K = 50, 100,$ and 200 for the wet bed case 47
5.11	The RMS error using $N = 1$ and $N = 2$ with $K = 25, 50,$ and 100 for the dry bed case 48
5.12	The RMS error using $N = 1$ and $N = 2$ with $K = 50, 100,$ and 200 and $(\theta_1, \theta_2) = (0.005, 0.0025)$ for the wet bed case, error indicator is applied 52
5.13	The RMS error using $N = 1$ and $N = 2$ with $K = 50, 100,$ and 200 $(\theta_1, \theta_2) = (0.005, 0.0025)$ for the wet bed problem, gradient indicator is applied 54

- 5.14 The RMS error using $N = 1$ and $N = 2$ with $K = 25, 50,$ and 100
and $(\theta_1, \theta_2) = (0.005, 0.0025)$ for the dry bed case, error indicator
is applied 57
- 5.15 The RMS error using $N = 1$ and $N = 2$ with $K = 25, 50,$ and $100,$
 $(\theta_1, \theta_2) = (0.005, 0.0025)$ for the dry bed problem, gradient indicator
is applied 60

LIST OF FIGURES

FIGURE	page
2.1 One-dimensional control volume	6
5.1 The comparison between the exact solution and the approximate solution obtained by the RKDG method at the final time $T = 1$ when $N = 2$ and $K = 160$	28
5.2 The log-log between the RMS errors and cell sizes for fix $N = 1, 2,$ and 3	29
5.3 The comparison between the exact solution and the approximate solution at the final time $T = 1$ when $N = 1$ and $K = 160$	31
5.4 The comparison of the exact solution and the numerical solution at the final time $T = 1$ using error indicator	33
5.5 The $x - t$ plot shows adaptive polynomial method from degree 1 to degree 3	33
5.6 The relationship between $\log(\text{RMS error})$ and $\log(K)$ for various values of θ_1 and θ_2 when $\text{mindeg}=1$ and $\text{maxdeg} = 3$, error indicator is applied. Number of cells are $K = 50, 100,$ and 200	35
5.7 The comparison of the exact solution with the numerical solution at the final time $T = 1$, using gradient indicator	36
5.8 The $x - t$ plot shows adaptive polynomial cells from degree 1 to degree 3	36
5.9 The relationship between $\log(\text{RMS error})$ and $\log(K)$ for various values of θ_1 and θ_2 when $\text{mindeg} = 1$ and $\text{maxdeg} = 3$, gradient indicator is applied. Number of cells are $K = 50, 100,$ and 200	37
5.10 The comparisons between the exact solution (dot line) and the numerical solution (solid line) at the final time $T = 1$, using error indicator in the adaptive mesh method for four cases of maxlev : $\text{maxlev} = 1$ (top-left), $\text{maxlev} = 2$ (top-right), $\text{maxlev} = 3$ (bottom left), and $\text{maxlev} = 4$ (bottom-right)	39

5.11	The relationship between RMS error and (θ_1, θ_2) when using $N = 1$ as basis function. Error indicator is applied where $K = 100$	40
5.12	The relationship between RMS error and (θ_1, θ_2) when using $N = 2$ as basis function. Error indicator is applied where $K = 100$	41
5.13	The comparisons between the exact solution (dot line) and the numerical solution (solid line) at the final time $T = 1$, using gradient indicator in the adaptive mesh method for four cases of <i>maxlev</i> : <i>maxlev</i> = 1 (top-left), <i>maxlev</i> = 2 (top-right), <i>maxlev</i> = 3 (bottom left), and <i>maxlev</i> = 4 (bottom-right)	42
5.14	The adaptive area for $N = 1$, $K = 100$, $(\theta_1, \theta_2) = (0.1, 0.05)$ (top) and $(\theta_1, \theta_2) = (0.025, 0.01)$ (bottom) with gradient indicator	44
5.15	The comparison between the exact solution and the numerical solution at final time $T = 1$ using $N = 1$ and $K = 200$ for the wet bed case	47
5.16	The comparison between the exact solution and the numerical solution at the final time $T = 1$ using $N = 1$ and $K = 100$ for wet bed case	48
5.17	The comparisons between the exact solution (solid line) and the approximate solution (dot line) for the wet bed at the final time $T = 1$, using error indicator in the adaptive mesh method for two cases of <i>maxlev</i> : <i>maxlev</i> = 1 (top) and <i>maxlev</i> = 2 (bottom)	50
5.18	The adaptive area for $N = 1$, $K = 100$, $(\theta_1, \theta_2) = (0.005, 0.0025)$ for <i>maxlev</i> = 1 (top) and <i>maxlev</i> = 2 (bottom) using error indicator	51
5.19	The comparisons between the exact solution(solid line) and the numerical solution(dot line) for the wet bed problem at the final time $T = 1$, using the gradient indicator in the adaptive mesh method for two cases of <i>maxlev</i> : <i>maxlev</i> = 1 (top) and <i>maxlev</i> = 2 (bottom) ..	52
5.20	The adaptive area for $N = 1$, $K = 100$, and $(\theta_1, \theta_2) = (0.005, 0.0025)$ for <i>maxlev</i> = 1 (top) and <i>maxlev</i> = 2 (bottom), when the gradient indicator is applied	53
5.21	The comparisons between the exact solution (solid line) and the approximate solution (dot line) for the dry bed problem at the final time $T = 1$, using error indicator in the adaptive mesh method	

	for two cases of <i>maxlev</i> : <i>maxlev</i> = 1 (top) and <i>maxlev</i> = 2 (bottom) ..	55
5.22	The adaptive area for $N = 1$, $K = 100$, and $(\theta_1, \theta_2) = (0.005, 0.0025)$ for <i>maxlev</i> = 1 (top) and <i>maxlev</i> = 2 (bottom) for error indicator	56
5.23	The comparisons between the exact solution (solid line) and the numerical solution (dot line) for dry bed problem at the final time $T = 1$, using gradient indicator in the adaptive mesh method for two cases of <i>maxlev</i> : <i>maxlev</i> = 1 (top) and <i>maxlev</i> = 2 (bottom)	58
5.24	The adaptive area for $N = 1$, $K = 100$, and $(\theta_1, \theta_2) = (0.005, 0.0025)$ for <i>maxlev</i> = 1 (top) and <i>maxlev</i> = 2 (bottom) with the gradient indicator is applied	59

CHAPTER I

INTRODUCTION

Many real flow problems such as transport flows or shallow water flows, for examples, can be expressed in the form of conservation laws. These systems are usually represented as hyperbolic partial differential equations. There are numerous numerical methods, for instance, the finite difference method (FDM) [1], the finite element method (FEM) [18], the finite volume method (FVM) [10, 16], or recently, the discontinuous Galerkin method (DG) [13, 15] for solving these systems. By the FDM, A. Harten and H. Tal-Ezer [1] presented a family of two-level five-point implicit schemes to solve the one-dimensional systems of hyperbolic conservation laws, which generalized the Crank-Nicholson scheme to the fourth order accuracy in both space and time. For the finite element method, Z. Xu et. al [18] applied the h-adaptive streamline diffusion finite element method with a small mesh-dependent artificial viscosity to solve nonlinear hyperbolic conservation equations. By applying the finite volume method, G. Manzini [10] developed the cell-centered upwind differences to solve the one-dimensional linear conservation laws with stiff reaction source terms. More details of the FVM can be found in Leveque, [16].

Conservation laws is an important class of homogeneous hyperbolic equation. The simplest case is when we have constant coefficients in one dimension, namely a scalar problem, in this case the equation is called the advection equation. Advection equation is an example of equation in conservative form that has various kinds of behaviors. For example, a weak solution can be in the form of a shock wave, namely, a solution that has a sharp gradient. For the case of system of equations, the shallow water equations are also in conservation forms which can be used to model many problems in real world such as dam break, tsunami, flood, etc. These equations can be derived from the conservation of mass and the conservation of momentum. We will give details of conservation laws and derivation of the shallow

water equations in Chapter II.

The finite element method can be used to solve these equations but the scheme has some limitations. We require to use very large number of nodes (for higher polynomial degrees or smaller mesh sizes) in order to obtain high accuracy solution, causing to use very massive computational time. In addition, this method usually does not preserve conservation property. However, the finite volume method is represented in conservation form, but generally only provide just second order of accuracy. Also increasing the order of approximation in each cell volume is difficult. The Discontinuous Galerkin (DG) method combining the FEM and FVM concepts, is then introduced to solve such the problem. The approximate solutions in any two cell volumes in the DG method need not to be equal at cell interface. The accuracy of approximate solutions depend on type of basis in each cell volume. Generally the polynomial basis is applied, so, the order of approximate solution is depend directly on the order of polynomial basis. The approximation in time derivative can be performed by the total variation diminishing Runge-Kutta (TVD-RK) method. Adjustment of the usual DG method to the Runge-Kutta discontinuous Galerkin (RKDG) method was first introduced by B. Cockburn, C.W. Shu [2, 3]. This method is employed to enforce the stability and convergence of numerical solution in time. The details of DG method for one dimensional scalar conservation laws [13, 15] and shallow water equations [6, 15] are discussed in Chapter III. The RKDG method has several advantages. It can be used to handle complex geometries, and also adaptivity strategies are easily applied since grid refinement can be done without taking into account the continuity condition that is typically required by most conforming finite element methods. Moreover, the degree of approximating polynomials can be adjusted locally, which allows an efficient polynomial adaptivity in each cell volume with totally independenceaa of its neighbors. Since we want to improve the accuracy of numerical solutions, especially locally in the sharp gradient area in the computational domain, we present two strategies that can overcome these issues, the adaptive polynomial degree, [9], and the adaptive mesh, [11], described in Chapter IV. We apply these two concepts and construct algorithms for the adaptive strategies employing two

types of indicators, the error and gradient indicators, for detecting troubled cells in the computational domain during time marching. For our preliminary work, we employ this presented method for the one-dimensional advection equation to observe the reliability and efficiency of the presented algorithms, and then apply these strategies to solve the one-dimensional shallow water equations. Note that for shallow water equations, we only apply adaptive mesh criteria. The numerical results of the advection equation and the shallow water equations from various techniques are presented in Chapter V. Finally, conclusions are given in Chapter VI.

CHAPTER II

DERIVATION OF SHALLOW WATER EQUATIONS

The shallow water equations (SWE, also called Saint Venant equations) are considered as system of hyperbolic partial differential equations that describe the flow below a pressure surface of a fluid. These equations are simplified from the Navier–Stokes equations, in the case where the horizontal length scale is much greater than the vertical length scale. In this thesis, we assumed that the flow is strictly one-dimensional and can be derived from the basic principles of conservation of mass and momentum. In this chapter, the conservation laws are first presented, and the derivation of the shallow water equations are shown later.

2.1 Conservation Laws

In these thesis, we consider hyperbolic equation of conservation laws, represented in the time dependent problem. In one dimensional case the equation takes the form

$$\frac{\partial}{\partial t}U(x, t) + \frac{\partial}{\partial x}F(U(x, t)) = 0, \quad (2.1)$$

where U is an m -dimensional vector of conserved quantities (or state variables), such as mass, momentum, or energy, in a fluid dynamic problem, $F(U)$ is an m -dimensional vector called the flux function.

To solve equation (2.1), some initial conditions and possibly boundary conditions on a bounded domain must be specified. The simplest case is the pure initial value problem, called the Cauchy problem, in which (2.1) holds for $-\infty < x < \infty$ and $t \geq 0$. We set the initial conditions as

$$U(x, 0) = U_0(x), \quad -\infty < x < \infty.$$

We also assumed the hyperbolic assumption on $F(U)$, namely, for each value of U the eigenvalues of the $m \times m$ Jacobian matrix $F'(U)$ of the flux function are real, and the matrix is diagonalizable, i.e., there is a complete set of m linearly independent eigenvectors.

The advection equation

$$\frac{\partial u}{\partial t} + c \frac{\partial u}{\partial x} = 0$$

is an example of equation in conservation form (2.1), this equation is a scalar equation in which $m = 1$ where $U = u(x, t)$ and $F(U) = cu$ where c constant. It is well-known that the solution from this equation has the same shape as the initial condition, and it advects along the horizontal direction with speed c . For example, if the initial condition has a shock (a singularity or discontinuity solution at a point of x), then the resulting solution will have a shock advects with speed c . Another system in conservation form is the shallow water equations

$$\frac{\partial h}{\partial t} + \frac{\partial q}{\partial x} = 0,$$

$$\frac{\partial q}{\partial t} + \frac{\partial}{\partial x} \left(\frac{q^2}{h} + \frac{gh^2}{2} \right) = 0.$$

The system is in conservation form in which $m = 2$, where

$$U = \begin{pmatrix} h \\ q \end{pmatrix}, F(U) = \begin{pmatrix} q \\ q^2/h + gh^2/2 \end{pmatrix}. \quad (2.2)$$

The derivation of these equations are given below.

2.2 Derivation of shallow water equations

The SWE can be derived from the basic principles of conservation of mass and momentum subject to the following assumptions:

- 1) The fluid is assumed to be incompressible and inviscid.
- 2) The fluid is nonturbulence flow.

3) The pressure distribution is hydrostatic.

The derivation of the conservation of mass and momentum for open-channel flow can be obtained from a consideration of the one-dimensional control volume as shown in the following figure.

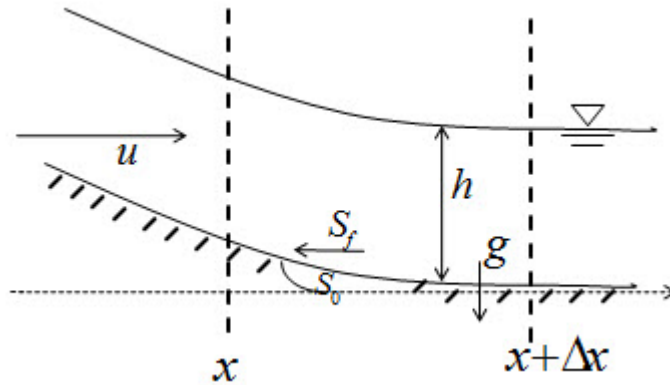


Figure 2.1: One-dimensional control volume

2.3 Conservation of mass

The principle of conservation of mass states

$$\boxed{\text{The rate of mass increase within the control volume}} = \boxed{\text{Mass flux entering the control volume}} - \boxed{\text{Mass flux leaving the control volume}}$$

Assume that the fluid is incompressible (the density of fluid ρ is constant). We denote the fluid depth and flow velocity in the x -direction by $h(x, t)$ and $u(x, t)$ respectively.

The mass flux entering the control volume at (x, t) is

$$\rho hu. \tag{2.3}$$

The mass flux leaving the control volume at $(x + \Delta x, t)$ is

$$\rho hu + \Delta x \frac{\partial}{\partial x} (\rho hu). \quad (2.4)$$

Then, the net rate of mass flux entering the control volume is

$$\rho hu - \left[\rho hu + \Delta x \frac{\partial}{\partial x} (\rho hu) \right] = -\Delta x \frac{\partial}{\partial x} (\rho hu). \quad (2.5)$$

The rate of mass increase within the control volume is

$$\Delta x \frac{\partial}{\partial t} (\rho h). \quad (2.6)$$

From (2.5) and (2.6) with the law of conservation of mass, the equation yields

$$\Delta x \frac{\partial}{\partial t} (\rho h) = -\Delta x \frac{\partial}{\partial x} (\rho hu). \quad (2.7)$$

Assuming that ρ is constant and dividing both sides of the equation by $\rho \Delta x$, we obtain

$$\frac{\partial h}{\partial t} = -\frac{\partial}{\partial x} (hu), \quad (2.8)$$

or

$$\frac{\partial h}{\partial t} + \frac{\partial}{\partial x} (hu) = 0. \quad (2.9)$$

Equation 2.9 is the conservation of mass equation in the one-dimensional shallow water equations.

2.4 Conservation of momentum

The principle of conservation of momentum states that

The rate of change of momentum in the control volume	=	The net rate of momentum flux entering the control volume	+	Sum of force acting on the control volume
--	---	---	---	---

The rate of momentum entering the control volume at (x, t) is the product of the mass flow rate and the velocity, i.e.,

$$\rho u^2 h, \quad (2.10)$$

and the momentum leaving the control volume at $(x + \Delta x, t)$ is

$$\rho u^2 h + \Delta x \frac{\partial}{\partial x} (\rho u^2 h). \quad (2.11)$$

Then, the net rate at which momentum enters the control volume is

$$\rho u^2 h - \left[\rho u^2 h + \Delta x \frac{\partial}{\partial x} (\rho u^2 h) \right] = -\Delta x \frac{\partial}{\partial x} (\rho u^2 h). \quad (2.12)$$

The forces acting on the control volume are as follows:

(1) The gravity force.

The body force due to the gravity is the weight of the fluid within the control volume acting in the direction of x -axis,

$$F_g = \rho g h \Delta x S_0, \quad (2.13)$$

where g is the acceleration due to gravity, and $S_0 = \sin \theta$ is the bed slope, which θ is the angle between the bottom and the x -axis along the channel. For small bed slope, $\sin \theta \approx \theta$.

(2) The hydrostatic pressure force.

The pressure force on vertical section of unit width and water depth h at (x, t) is

$$F_p|_x = \int_0^h \rho g (h - y) dy = \frac{1}{2} \rho g h^2. \quad (2.14)$$

The pressure force on vertical section of unit width and water depth h at $(x + \Delta x, t)$ is

$$F_p|_{x+\Delta x} = \frac{1}{2} \rho g h^2 + \Delta x \frac{\partial}{\partial x} \left(\frac{1}{2} \rho g h^2 \right). \quad (2.15)$$

The net of pressure force on two vertical side to the x -direction is

$$\frac{1}{2}\rho gh^2 - \left[\frac{1}{2}\rho gh^2 + \Delta x \frac{\partial}{\partial x} \left(\frac{1}{2}\rho gh^2 \right) \right] = -\frac{\Delta x}{2} \frac{\partial}{\partial x} (\rho gh^2). \quad (2.16)$$

(3) The frictional force.

The frictional force which is assumed to act on the bottom and the sides of the channel is given by

$$F_f = \rho gh \Delta x S_f, \quad (2.17)$$

where S_f is the friction slope. The term S_f can be estimated by an empirical formulae, and in this work, we employed the Manning resistance law represented by

$$S_f = \frac{n^2 uh |uh|}{h^{10/3}}, \quad (2.18)$$

where n is the Manning roughness coefficient.

The rate of change of the momentum in the control volume is

$$\Delta x \frac{\partial}{\partial t} (\rho uh). \quad (2.19)$$

Combining (2.12), (2.13), (2.14), (2.17) and (2.19), with the law of conservation of momentum, the equation yields

$$\Delta x \frac{\partial}{\partial t} (\rho uh) = -\Delta x \frac{\partial}{\partial x} (\rho u^2 h) + gh \rho \Delta x (S_0 - S_f) - \frac{g}{2} \Delta x \frac{\partial (\rho h^2)}{\partial x}. \quad (2.20)$$

Assuming that ρ is constant and dividing both sides of the equation by $\rho \Delta x$, we obtain

$$\frac{\partial}{\partial t} (uh) = -\frac{\partial}{\partial x} (u^2 h) + gh (S_0 - S_f) - \frac{g}{2} \frac{\partial h^2}{\partial x}, \quad (2.21)$$

and can be rewritten as

$$\frac{\partial}{\partial t} (uh) + \frac{\partial}{\partial x} \left(u^2 h + \frac{gh^2}{2} \right) = gh (S_0 - S_f). \quad (2.22)$$

Since the quantity hu is often call the discharge q , measuring the flow rate of water at a certain point in space, then (2.9) and (2.22) can be rewritten as

$$\frac{\partial h}{\partial t} + \frac{\partial q}{\partial x} = 0, \quad (2.23)$$

$$\frac{\partial q}{\partial t} + \frac{\partial}{\partial x} \left(\frac{q^2}{h} + \frac{gh^2}{2} \right) = gh(S_0 - S_f), \quad (2.24)$$

which give the shallow water equations.

The system in the conservation form (2.1) is obtained by setting source term

$$S(U) = \begin{pmatrix} 0 \\ gh(S_0 - S_f) \end{pmatrix} = 0, \quad (2.25)$$

and

$$U = \begin{pmatrix} h \\ q \end{pmatrix}, \quad F(U) = \begin{pmatrix} q \\ q^2/h + gh^2/2 \end{pmatrix}. \quad (2.26)$$

CHAPTER III

NUMERICAL METHOD

In this chapter, we presented the Discontinuous Galerkin method for solving the one-dimensional scalar conservation law and the shallow water equations.

3.1 The Discontinuous Galerkin (DG) scheme for the one-dimensional scalar conservation law

The one-dimensional scalar conservation law is in the form

$$u_t + f(u)_x = 0, \quad (3.1)$$

$$u(x, 0) = u_0(x), \quad (3.2)$$

where $x \in (a, b)$ and $t \in (0, T)$, for some fixed T .

In this thesis, we considered the advection equation which is also in the conservation form, where $f(u) = cu$ and c is a constant.

First we partition the domain (a, b) into K subintervals, and denoted the j -th cell by $I_j = [x_{j-1/2}, x_{j+1/2}]$, $j = 1, \dots, K$ with the grid size $\Delta_j = x_{j+1/2} - x_{j-1/2}$ and the cell center is $x_j = (x_{j+1/2} + x_{j-1/2})/2$, where $x_{j+1/2}$ and $x_{j-1/2}$ are the left and the right boundaries of the cell, respectively.

Approximating the solution u by u_h in the finite dimensional space V_h^N defined by

$$V_h^N = \{v \in L^1(0, 1) : v|_{I_j} \in P^N(I_j), j = 1, \dots, K\}, \quad (3.3)$$

where $P^N(I_j)$ denotes the space of polynomials of degree at most N on I_j , and $L^1(0, 1)$ is the space of integrable functions on $[0, 1]$

Multiplying (3.1) and (3.2) by a test function $v_h(x) \in P^N(I_j) \subset V_h^N|_{I_j}$ and using the integration by parts over I_j , we obtain (weak form),

$$\int_{I_j} (\partial_t u_h) v_h dx - \int_{I_j} f(u_h) \partial_x v dx + [f(u_h) v_h]_{j+\frac{1}{2}} - [f(u_h) v_h]_{j-\frac{1}{2}} = 0, \quad (3.4)$$

$$\int_{I_j} u(x, 0) v(x) dx = \int_{I_j} u_0(x) v(x) dx, \quad j = 1, \dots, K. \quad (3.5)$$

The flux function f can be approximated using numerical flux \hat{f} that depends on the two values of u_h at the interfaces $x_{j\pm\frac{1}{2}}$ by

$$\hat{f}_{j+\frac{1}{2}} = \hat{f}(u_h|_{j+\frac{1}{2}}^-, u_h|_{j+\frac{1}{2}}^+), \quad \hat{f}_{j-\frac{1}{2}} = \hat{f}(u_h|_{j-\frac{1}{2}}^-, u_h|_{j-\frac{1}{2}}^+). \quad (3.6)$$

The notations $u_h|_{j\pm\frac{1}{2}}^-$ and $u_h|_{j\pm\frac{1}{2}}^+$ are the approximate solution from the left and right of the boundaries $j\pm\frac{1}{2}$ of the j -th cell, respectively. By choosing the Legendre polynomials P_m , defined on $[-1, 1]$ as the local basis functions, the approximate solution u_h can be written as

$$u_h(x, t)|_{I_j} = \sum_{m=0}^N u_j^m(t) \varphi_m(x), \quad (3.7)$$

where $u_j^m(t)$ is the coefficient function of t , and $\varphi_m(x)$ is the Legendre polynomial defined by

$$\varphi_m(x) = P_m\left(\frac{2(x-x_j)}{\Delta_j}\right). \quad (3.8)$$

As in the standard Galerkin method, we choose the test functions $v_h(x)$ to be the same as the basis functions, i.e., $v_h(x) = \{\varphi_l(x)\}_{l=0}^N$. Some important properties of the Legendre's polynomial are

$$\int_{-1}^1 P_m(\xi) P_l(\xi) d\xi = \frac{2}{2l+1} \delta_{ml}, \quad (3.9)$$

where

$$\xi = \frac{2(x - x_j)}{\Delta_j}, \quad \delta_{ml} = \begin{cases} 1, & m = l \\ 0, & m \neq l \end{cases}, \quad (3.10)$$

and

$$P_l(-1) = (-1)^l, \quad P_l(1) = 1. \quad (3.11)$$

The weak forms (3.4) and (3.5) are then simplified to a semidiscrete ODE,

$$\frac{du_j^l(t)}{dt} = \frac{2l+1}{\Delta_j} \int_{I_j} f(u_h) \partial_x \varphi_l(x) dx + \frac{2l+1}{\Delta_j} \left\{ (-1)^l \hat{f}_{j-\frac{1}{2}} - \hat{f}_{j+\frac{1}{2}} \right\}, \quad (3.12)$$

$$u_j^l(0) = \frac{2l+1}{\Delta_j} \int_{I_j} u(x, 0) \varphi_l(x) dx, \quad (3.13)$$

for $j = 1, \dots, K$ and $l = 1, \dots, N$.

3.1.1 Convergence analysis of linear case

In the advection case $f(u) = cu$, we have the following theorems[2].

Theorem 3.1. *Suppose that the initial condition u_0 belong to Sobolev space $H^{N+1}(0, 1)$.*

Let e be the error $u - u_h$. Then we have,

$$\|e(T)\|_{L^2(0,1)} \leq C |u_0|_{H^{N+1}(0,1)} (\Delta x)^{N+1/2},$$

where C depend solely on N , $|c|$, and T .

If we assume that the initial condition is more regular, then we have the following result.

Theorem 3.2. *Suppose that the initial condition u_0 belong to Sobolev space $H^{N+2}(0, 1)$.*

Let e be the error $u - u_h$. Then we have

$$\|e(T)\|_{L^2(0,1)} \leq C |u_0|_{H^{N+2}(0,1)} (\Delta x)^{N+1},$$

where C depend solely on N , $|c|$, and T .

Theorem 3.1 is a simplified version of a more general result proven by Johnson and Pitkäranta in 1986 and Theorem 3.2 is a simplified version of a more general result proven by Lesaint and Raviart in 1974. Proofs of Theorems 3.1 and 3.2 can be found in [2].

The above theorems show that the DG scheme is $(N + 1)$ th-order accurate scheme, at least in the advection case, provided that the regularity assumption is met as stated in the theorems. In addition, the same order of accuracy should still hold in the nonlinear case when the exact solution is smooth enough, see details in [2].

3.1.2 Numerical flux

The DG scheme is called monotone if the function $\hat{f}(\alpha, \beta)$ is Lipschitz continuous, consistent and monotone, in the sense that,

- (i) \hat{f} is locally Lipschitz and consistent with the flux $f(u)$, i.e., $\hat{f}(u, u) = f(u)$;
- (ii) \hat{f} is nondecreasing in its first argument; and
- (iii) \hat{f} is nonincreasing in its second argument.

In this thesis, we employ the local Lax-Friedrichs flux that satisfies the above properties, represented by

$$\hat{f}(\alpha, \beta) = \frac{1}{2} [f(\alpha) + f(\beta) - C(\beta - \alpha)] , \quad (3.14)$$

where $C = \max |f'(s)|$, $\min(\alpha, \beta) \leq s \leq \max(\alpha, \beta)$.

3.1.3 Total Variation Diminishing Runge Kutta (TVD-RK)

After discretizing (3.1) and (3.2) in spatial space by the DG method, we obtain a system of ODEs corresponding to (3.12) and (3.13). The system can be rewritten in the form of

$$\frac{du_h(t)}{dt} = L_h(u_h, t), \quad \forall t \in (0, T), \quad (3.15)$$

with

$$u_h(x, 0) = u_{0h}, \quad (3.16)$$

where $L_h(u_h, t)$ represents the right hand side of equation (3.12).

The time discretization process is done by the high-order TVD Runge Kutta method which was introduced previously by Chi-Wang Shu [1988]. Noted that when polynomial degree N is used, a TVD version of Runge Kutta method at least of order $N + 1$ must be employed in order to obtain solution accuracy as stated in theorems 3.1 and 3.2.

Let $\{t^n\}_{n=0}^M$ are a partition of $[0, T]$ in M intervals, and $\Delta t^n = t^{n+1} - t^n$, for $n = 0, \dots, M - 1$. The time marching algorithm can be summarized as follows.

1. Set $u_h^0 = u_{0h}$,
2. For $n = 0, \dots, M - 1$ compute u_h^{n+1} from u_h^n as follows:
3. set $d^{(0)} = u_h^n$,
4. for $i = 1, \dots, k + 1$ compute the intermediate functions:

$$d^{(i)} = \left\{ \sum_{s=0}^{i-1} (\alpha_{is} d^{(s)} + \beta_{is} \Delta t^n L_h(d^{(s)}, t)) \right\},$$

5. set $u_h^{n+1} = d^{(k+1)}$,

where α_{is} and β_{is} are parameters depend on the order of TVD-RK.

For example, the TVD-RK of orders 2 and 3 are given by

TVD-RK order 2

$$d^{(1)} = u_h^n + L_h(u_h^n, t^n), \quad (3.17)$$

$$u_h^{n+1} = d^{(2)} = \frac{1}{2} (u_h^n + d^{(1)} + \Delta t L_h(d^{(1)}, t^n + \Delta t)), \quad (3.18)$$

TVD-RK order 3

$$d^{(1)} = u_h^n + \Delta t L_h(u_h^n, t^n), \quad (3.19)$$

$$d^{(2)} = \frac{1}{4} (3u_h^n + d^{(1)} + \Delta t L_h(d^{(1)}, t^n + \Delta t)), \quad (3.20)$$

$$u_h^{n+1} = \frac{1}{3} \left(u_h^n + 2d^{(2)} + 2\Delta t L_h \left(d^{(2)}, t^n + \frac{1}{2}\Delta t \right) \right). \quad (3.21)$$

By these setting, the TVD-RK has some useful stability properties. Details can be seen in [2, 13].

3.1.4 The MUSCL slope limiter

When high-order polynomials are used for approximating the solution, numerical method may produce some unphysical oscillations [2, 6, 13, 15, 16]. A slope limiter concept can be applied on every computational cell to avoid these undesired oscillations. For instance, in the case of piecewise linear approximation, the slope limiter of $u_h|_{I_j}$ is denoted by $\Lambda \Pi_h^1(u_h|_{I_j})$

$$\Lambda \Pi_h^1(u_h|_{I_j}) = \bar{u}_j + (x - x_j) m \left(u_{x,j}, \frac{\bar{u}_{j+1} - \bar{u}_j}{\Delta_j}, \frac{\bar{u}_j - \bar{u}_{j-1}}{\Delta_j} \right), \quad (3.22)$$

for $j = 1, \dots, K$.

In (3.22) \bar{u}_j is the mean value in the j -th cell, $u_{x,j}$ is the slope of solution in the j -th cell, and m is the minmod function defined by

$$m(a_1, a_2, \dots, a_n) = \begin{cases} \text{sign}(a_1) \min_{1 \leq i \leq n} |a_i|, & \text{if } \text{sign}(a_1) = \dots = \text{sign}(a_n), \\ 0, & \text{otherwise.} \end{cases} \quad (3.23)$$

This is the well-known slope limiter of the MUSCL schemes introduced by vanLeer[4, 5].

In the case that the approximate solution is a polynomial degree $N \geq 2$, that is,

$$u_h|_{I_j}(x, t) = \sum_{l=0}^N u_j^l(t) \varphi_l(x) .$$

We defined what could be called the P^1 -part of u_h denoted by u_h^1 as

$$u_h^1|_{I_j}(x, t) = \sum_{l=0}^1 u_j^l(t) \varphi_l(x) .$$

The slope limiter procedure in this case denoted by $\Lambda\Pi_h^N$, is summarized as follows:

- (1) Compute $\tilde{u}_{j+\frac{1}{2}}^-$ and $\tilde{u}_{j-\frac{1}{2}}^+$ from

$$\tilde{u}_{j+\frac{1}{2}}^- = \bar{u}_j + m \left(u_{j+\frac{1}{2}}^- - \bar{u}_j, \bar{u}_j - \bar{u}_{j-1}, \bar{u}_{j+1} - \bar{u}_j \right) , \quad (3.24)$$

$$\tilde{u}_{j-\frac{1}{2}}^+ = \bar{u}_j - m \left(\bar{u}_j - u_{j-\frac{1}{2}}^+, \bar{u}_j - \bar{u}_{j-1}, \bar{u}_{j+1} - \bar{u}_j \right) . \quad (3.25)$$

- (2) If $\tilde{u}_{j+\frac{1}{2}}^- = u_{j+\frac{1}{2}}^-$ and $\tilde{u}_{j-\frac{1}{2}}^+ = u_{j-\frac{1}{2}}^+$ set $\Lambda\Pi_h^N(u_h|_{I_j}) = u_h|_{I_j}$.
(3) Otherwise, take $u_h|_{I_j}$ equal to $\Lambda\Pi_h^1(u_h^1|_{I_j})$.

3.2 Discontinuous Galerkin method for the one-dimensional shallow water equations

Next, we introduced the RKDG method for solving the one-dimensional shallow water equations in this form

$$\frac{\partial U}{\partial t} + \frac{\partial F(U)}{\partial x} = S(U) , \quad (3.26)$$

where $x \in (0, L)$ and $t \in (0, T)$, with

$$U = \begin{pmatrix} h \\ q \end{pmatrix}, \quad F(U) = \begin{pmatrix} q \\ q^2/h + gh^2/2 \end{pmatrix} \quad (3.27)$$

are the vector of conserve variables and the flux vector in the x direction, respectively, t is the time, h is the water depth, u is the flow velocity in the x -direction, $q = uh$ is the discharge, and g is the acceleration due to gravity.

The right hand side of the system (3.26) represents the source term, given by

$$S(U) = \begin{pmatrix} 0 \\ gh(S_0 - S_f) \end{pmatrix}, \quad (3.28)$$

which contains the effect of the bed slope S_0 , and the bed friction S_f . The term S_f can be estimated by an empirical formulae as

$$S_f = \frac{n^2 q |q|}{h^{10/3}}, \quad (3.29)$$

where n is the Manning roughness coefficient.

In this thesis, we neglect the effect of source term, so $S(U) = 0$. We then investigate the efficiency of the DG method for solving the shallow water equations without source term treatment.

Similar to the one-dimensional scalar conservation case, we first partition the domain $(0, L)$ into K subintervals, and denoted the j -th cell by $I_j = [x_{j-1/2}, x_{j+1/2}]$, $j = 1, \dots, K$, with the grid size $\Delta_j = x_{j+1/2} - x_{j-1/2}$, and the cell center $x_j = (x_{j+1/2} + x_{j-1/2})/2$, $x_{j+1/2}$ and $x_{j-1/2}$ are the left and right boundaries of the considering cell respectively.

Again, approximating the solution U by $U_h = \begin{pmatrix} h_h \\ q_h \end{pmatrix}$ in the finite dimensional space, $V_h^N \times V_h^N$.

Multiplying (3.26) by a test function $v_h(x) \in P^N(I_j)$ and using the integration by parts over I_j , we obtain a weak form,

$$\int_{I_j} (\partial_t U_h) v_h dx - \int_{I_j} F(U_h) \partial_x v_h dx + [F(U_h) v_h]_{j+1/2} - [F(U_h) v_h]_{j-1/2} = \int_{I_j} S(U_h) v_h dx. \quad (3.30)$$

The flux function F can be approximated using numerical flux \hat{F} that depends on the two values of U_h at the interfaces $x_{j\pm 1/2}$ by

$$\hat{F}_{j+\frac{1}{2}} = \hat{F} \left(U_h|_{j+\frac{1}{2}}^-, U_h|_{j+\frac{1}{2}}^+ \right), \quad \hat{F}_{j-\frac{1}{2}} = \hat{F} \left(U_h|_{j-\frac{1}{2}}^-, U_h|_{j-\frac{1}{2}}^+ \right), \quad (3.31)$$

where $U_h|_{j\pm\frac{1}{2}}^-$ and $U_h|_{j\pm\frac{1}{2}}^+$ are the approximate solution from the left and right of the boundaries $j \pm \frac{1}{2}$ of the j -th cell, respectively.

By choosing the Legendre polynomials P_m as the local basis functions, the approximate solution U_h can be written as

$$U_h(x, t) = \sum_{m=0}^N U_j^m(t) \varphi_m(x), \quad (3.32)$$

where $U_j^m(t)$ is the coefficient function of t , and $\varphi_m(x)$ is the Legendre polynomial which is defined as before.

The weak forms (3.30) are then simplified to

$$\begin{aligned} & \left(\frac{1}{2l+1} \right) \frac{dU_j^l(t)}{dt} - \frac{1}{\Delta_j} \int_{I_j} F(U_h) \varphi_l'(x) dx + \frac{1}{\Delta_j} \left\{ \hat{F}(U_h)_{j+\frac{1}{2}} - (-1)^l \hat{F}(U_h)_{j-\frac{1}{2}} \right\} \\ & = \frac{1}{\Delta_j} \int_{I_j} S(U_h) \varphi_l(x) dx, \end{aligned} \quad (3.33)$$

where $j = 1, \dots, K$.

3.2.1 Numerical flux

The DG scheme is monotone if $\hat{F}(U_L, U_R)$ is a Lipschitz, consistent and monotone flux in the sense as state in the one-dimensional scalar conservation case. For the shallow water equations, Toro [7, 8] presented a suitable HLL(Harten-Lax-van Leer)-type flux [6, 7, 8, 15] based on the work by Harten et. al.[1],

$$\hat{F}^{HLL}(U_L, U_R) = \begin{cases} F_L & \text{if } 0 \leq S_L; \\ F^* & \text{if } S_L \leq 0 \leq S_R; \\ F_R & \text{if } 0 \geq S_R, \end{cases} \quad (3.34)$$

where $F_L = F(U_L)$, $F_R = F(U_R)$, and F^* is given by

$$F^* = \frac{S_R F_L - S_L F_R + S_L S_R (U_R - U_L)}{S_R - S_L}. \quad (3.35)$$

The wave speeds are chosen under the assumption of two-rarefaction waves in the star region,

$$S_L = \min \left(u_L - \sqrt{gh_L}, u^* - \sqrt{gh^*} \right), \quad (3.36)$$

$$S_R = \min \left(u_R + \sqrt{gh_R}, u^* + \sqrt{gh^*} \right), \quad (3.37)$$

with

$$\sqrt{gh^*} = \frac{1}{2} \left(\sqrt{gh_L} + \sqrt{gh_R} \right) - \frac{1}{4} (u_R - u_L), \quad (3.38)$$

$$u^* = \frac{1}{2} (u_L + u_R) + \sqrt{gh_L} - \sqrt{gh_R}. \quad (3.39)$$

The expressions for the wave speeds are obtained by assuming the wet bed condition, i.e. positive flow depth h on both sides of the computational domain. For the dry bed case the wave speeds are approximated by

$$S_L = u_L - \sqrt{gh_L}, \quad (3.40)$$

and

$$S_R = u_L + 2\sqrt{gh_L}. \quad (3.41)$$

3.2.2 The TVD-RK time discretization and slope limiter for the SWE

Once the system has been discretized in the spatial space using the DG method, the system can be integrated forward in time by the TVD-RK method as described in section 3.1.3. As described earlier, the non-physical oscillations resulting from the space discretizations can be avoid by using the MUSCL slope limiter on every computational cell during time marching process performed.

CHAPTER IV

ADAPTIVE METHOD

In general, the accuracy of the approximate solution can be improved by increasing the degrees of polynomials of local basis functions in each cell or refine grid cells with smaller mesh size in the computational domain. But for efficiency of the computation, it should be adapted only for troubled cells area where the solutions have large error, sharp gradients, or discontinuities.

In this chapter, we presented two types of adaptive algorithms, adaptive polynomial and adaptive mesh. The adaptive polynomial is successfully applied for solving the case of initially smooth data by increasing order of polynomial basis while the adaptive mesh can be used to handle the case of high gradients or discontinuities. To detect which cell needed to be applied the adaptive criteria, we need some indicators to detect those troubled cells. In this thesis, we employed two type of indicators which are error indicator (assuming we know the exact solution) and gradient indicator.

4.1 Indicators

The values of the indicators for the j -th cell at time t^n , denoted by ε_j^n , are defined as follows:

(1) Error indicator

$$\varepsilon_j^n = \sqrt{\frac{\sum_{n_g} (q_{exact}^n - q_{approx}^n)^2}{n_g}}, \quad (4.1)$$

where q_{exact}^n is the exact solution, q_{approx}^n is an approximate solution, and n_g is the number of nodes on the j -th cell at time t^n . This indicator is the root mean square error (RMS error) in the j -th cell. Note that to compute the error indicator

ε_j^n , we need to know the exact solution of the problem.

(2) Gradient indicator

$$\varepsilon_{j,1}^n = \frac{|q_{approx}^n|_{j+\frac{1}{2}} - q_{0approx}^n|_j|}{\Delta_j/2}, \quad (4.2)$$

$$\varepsilon_{j,2}^n = \frac{|q_{approx}^n|_{j-\frac{1}{2}} - q_{0approx}^n|_j|}{\Delta_j/2}, \quad (4.3)$$

where $q_{approx}^n|_{j-\frac{1}{2}}$ and $q_{approx}^n|_{j+\frac{1}{2}}$ are approximate solutions for j -th cell at the left and right boundaries respectively, and $q_{0approx}^n|_j$ is approximate solution at the center of the j -th cell.

For general problems that the exact solution are not known, the gradient indicator can be applied instead of using the error indicator. In our adaptive technique, indicator is the most important quantity for detecting troubled cells, and gradient indicator would be a practical choice that is often used for conservation laws or SWE, see [9].

4.2 Adaptive polynomial for RKDG method (p-adaptive)

Algorithm for the adaptive polynomial

Given:

A control number for increasing the degree of polynomial, θ_1 .

A control number for decreasing the degree of polynomial, θ_2 .

The initial degree of polynomial, *mindeg*.

The maximum degree of polynomial, *maxdeg*.

The final time, T .

A partition of time domain $[0, T]$, $\{t^n\}_{n=0}^N$

Initial condition, u^0 at time step t^0 .

The number of cells, K .

The algorithm is summarized below:

Step 1.

1. Given a uniform partition of the domain.
2. Compute approximate solution u^1 at time step t^1 .
3. For each cell $j = 1, 2, \dots, K$,
 - set the initial degree of polynomial $deg_j^0 = mindeg$.

Step 2. Define the degree of polynomial in the j -th cell at time t^n by deg_j^n ,

1. Compute the indicator ε_j^n .
2. Set $max\varepsilon = \max_{1 \leq j \leq K} \{\varepsilon_j^n\}$. For each cell $j = 1, 2, \dots, K$,
 - error indicator case: If $\varepsilon_j^n > \theta_1 max\varepsilon$, mark this j -th cell as a troubled cell.
 - gradient indicator case: If $\varepsilon_{j,1}^n > \theta_1 max\varepsilon$ or $\varepsilon_{j,2}^n > \theta_1 max\varepsilon$, mark this j -th cell as a trouble cell
3. Increase the degree of polynomial of the mark cell.
 - If $deg_j^{n-1} = maxdeg$, do nothing.
 - If $deg_j^{n-1} < maxdeg$, set the new degree in that troubled cell as $deg_j^{n-1}|_{new} = deg_j^{n-1} + 1$.
4. For the current troubled cell at time t^n , $n \geq 1$
 - error indicator case: If $\varepsilon_j^n < \theta_2 max\varepsilon$, release this troubled cell as a usual cell.
 - gradient indicator case: If $\varepsilon_{j,1}^n < \theta_2 max\varepsilon$ and $\varepsilon_{j,2}^n < \theta_2 max\varepsilon$ release this troubled cell as a usual cell.

5. Decrease the degree of polynomial of usual cells.

- If the $deg_j^{n-1} = mindeg$, do nothing.
- If $deg_j^{n-1} > mindeg$, set the new degree as $deg_j^{n-1}|_{new} = deg_j^{n-1} - 1$.

In this step, we now have a new degree of polynomial for each cell at time t^{n-1} .

Step 3. Using L^2 -projection, project the temporal coefficients $\{u_j^l(t^{n-1})\}_{l=0}^{deg_j^{n-1}}$ to the new set of $\{u_j^l(t^{n-1})\}_{l=0}^{deg_j^{n-1}|_{new}}$.

Step 4. Evolve numerical solutions of all cells from t^{n-1} to t^n .

Step 5. If $n < N$, repeat the whole steps by going back to step 2.

4.3 Adaptive mesh for RKDG method (h-adaptive)

Since for shock or discontinuous solution, the high-order of polynomial approximation cannot improve the accuracy of numerical solution, the adaptive mesh criteria can be employed to increase the accuracy of solution for this case.

Algorithm for adaptive mesh

Given:

A control number used to divide troubled cell into two smaller cells, θ_1 .

A control number for merging untroubled cell into one cell, θ_2 .

The degree of polynomial, N .

The maximum level of mesh partition, $maxlev$.

The final time, T .

A partition of time domain $[0, T]$, $\{t^n\}_{n=0}^N$

Initial condition, u^0 at time step t^0 .

The initial number of cell K .

The algorithm is summarized below:

Step 1.

1. Given a uniform partition of the domain.
2. Compute approximate solution u^1 at time step t^1 .
3. For each cell $j = 1, 2, \dots, K$,
 - set the initial mesh level of every cell as $lev_j^0 = 0..$

Step 2. Define the mesh partition at time t^n and the mesh level for the j -th cell by $\{l^n\}$ and lev_j^n , respectively.

1. Compute the indicator ε_j^n .
2. Set $max\varepsilon = \max_{1 \leq j \leq K} \{\varepsilon_j^n\}$. For each cell $j = 1, 2, \dots, K$,
 - error indicator case: If $\varepsilon_j^n > \theta_1 max\varepsilon$, mark this j -th cell as a troubled cell.
 - gradient indicator case: If $\varepsilon_{j,1}^n > \theta_1 max\varepsilon$ or $\varepsilon_{j,2}^n > \theta_1 max\varepsilon$, mark this j -th cell as a trouble cell
3. Divide mark cells into two sub-cells.
 - If the $lev_j^{n-1} = maxlev$, do nothing.
 - If $lev_j^{n-1} < maxlev$, set new level as $lev_j^{n-1}|_{new} = lev_j^{n-1} + 1$, and divide it into two sub-cells.
4. For the current troubled cell at time t^n , $n \geq 1$
 - error indicator case: If $\varepsilon_j^n < \theta_2 max\varepsilon$, release this troubled cell as a usual cell.
 - gradient indicator case: If $\varepsilon_{j,1}^n < \theta_2 max\varepsilon$ and $\varepsilon_{j,2}^n < \theta_2 max\varepsilon$ release this troubled cell as a usual cell.

5. merge two usual cells into one cell.

- If $lev_j^{n-1} = 0$, do nothing.
- If $lev_j^{n-1} > 0$, set the new level to be $lev_j^{n-1}|_{new} = lev_j^{n-1} - 1$ and merge those two sub-cells into one cell (merge cells that come from the same primary cell).

This step provides the new mesh level for each cell at time t^{n-1} .

Step 3. Using L^2 -projection, project the temporal coefficients $\{u_j^l(t^{n-1})\}_{l=0}^N$ from the mesh partition $\{l^{n-1}\}$ to the new mesh partition $\{l^{n-1}\}|_{new}$.

Step 4. Evolve numerical solutions for every cells from t^{n-1} to t^n .

Step 5. If $n < N$, repeat the whole steps by going back to step 2.

CHAPTER V

NUMERICAL RESULTS AND DISCUSSIONS

The numerical results obtained by the adaptive Discontinuous Galerkin method for solving the advection equation and the shallow water equations are presented in this chapter.

5.1 Advection Equation

In this section, we will show some numerical results using the RKDG method (use as comparison), and the adaptive RKDG methods for both p-adaptive and h-adaptive. In these two adaptive cases, we applied two indicators as described in Chapter IV to detect the troubled cells in the computational domain.

The advection equation is

$$u_t + cu_x = 0, \quad (a,b) \times (0, T), \quad (5.1)$$

where c is a constant. The initial condition is

$$u(x, 0) = u_0(x). \quad (5.2)$$

The exact solution of this equation is

$$u(x, t) = u_0(x - ct). \quad (5.3)$$

The solution profile $u(x, t)$ is simply propagated by speed c with unchanged shape from initial data. Details for solving this equation can be seen in [13, 16, 17].

5.1.1 RKDG method without adaptive criteria for advection equation

First, we consider the pure advection equation with initially smooth condition as a model problem,

$$u_t + 3u_x = 0, \quad (-10,10) \times (0,1), \quad (5.4)$$

$$u(x,0) = e^{-(x-3)^2}. \quad (5.5)$$

In this case the exact solution is

$$u(x,t) = e^{-(x-3t-3)^2}. \quad (5.6)$$

The comparison between the exact solution and the approximate solution from the RKDG method is shown in Figure 5.1. It is shown that the approximate solution is in good agreement with the exact solution. Here we set the polynomial degree $N = 2$ and the number of cells $K = 160$

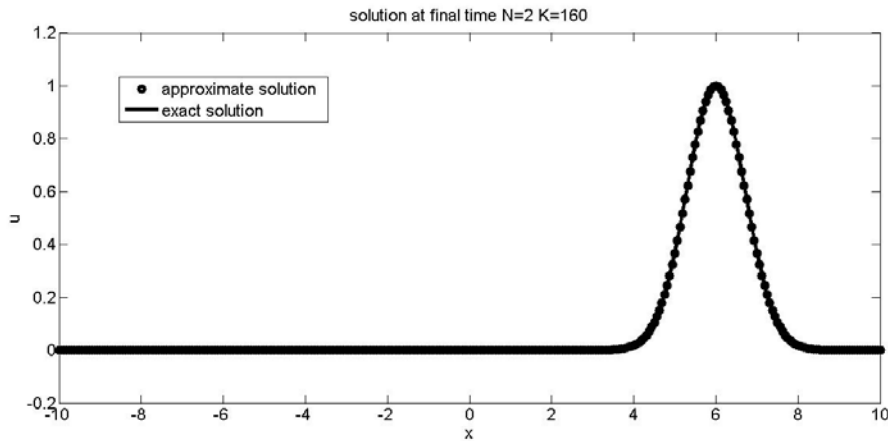


Figure 5.1: The comparison between the exact solution and the approximate solution obtained by the RKDG method at the final time $T = 1$ when $N = 2$ and $K = 160$.

The numerical results obtained by the RKDG method using polynomial degrees N of 1, 2 and 3, with the number of cells $K = 20, 40, 80,$ and 160 are shown in Table 5.1.

N/K	20	40	80	160	rate of convergent
1	5.4550×10^{-2}	1.3197×10^{-2}	2.7139×10^{-3}	5.9797×10^{-4}	2.2
2	7.7356×10^{-3}	1.1201×10^{-3}	1.4749×10^{-4}	1.8700×10^{-5}	2.9
3	6.9540×10^{-4}	9.0615×10^{-5}	6.2292×10^{-6}	3.9710×10^{-7}	3.6

Table 5.1: The RMS errors and rate of convergences when using the RKDG method for $N = 1, 2,$ and $3,$ and using $K = 20, 40, 80,$ and $160.$

The results in Table 5.1 show that the solutions obtained from the higher degree of polynomial are more accurate than using the lower degree of polynomial. For a fixed degree of polynomial, the accuracy of numerical solutions increase as the number of cell increases. These results are in expected and correspond with the theoretical results as provided in Theorem 3.2. The rates of convergence for the polynomial degree one, two and three are approximately in order of 2, 3 and 4 respectively. The log-log plot shown in Figure 5.2 also reveal these rates of convergence in term of the slope of straight line.

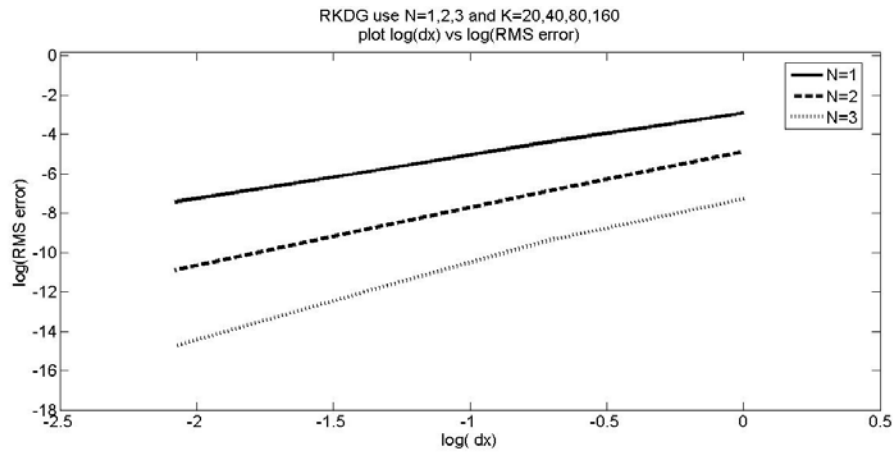


Figure 5.2: The log-log between the RMS errors and cell sizes for fix $N = 1, 2,$ and 3

Next, we consider the pure advection equation with discontinuous initial condition

$$u_t + 3u_x = 0, \quad (-10,10) \times (0,1) \quad (5.7)$$

$$u(x,0) = \begin{cases} 2, & \text{if } x \geq 2, \\ 1, & \text{if } x < 2. \end{cases} \quad (5.8)$$

The exact solution is

$$u(x,t) = \begin{cases} 2, & \text{if } x \geq 2 + 3t, \\ 1, & \text{if } x < 2 + 3t \end{cases} \quad (5.9)$$

The profile of numerical solution obtained by the RKDG method with the linear polynomial basis and the number of cells $K = 160$ is shown in Figure 5.3. It is found that the numerical solution is in good agreement with the exact solution. The speed of sharp-front or shock interface has been detected correctly by this method but there are some areas on the top and the bottom of shock that the method provides smear behavior.

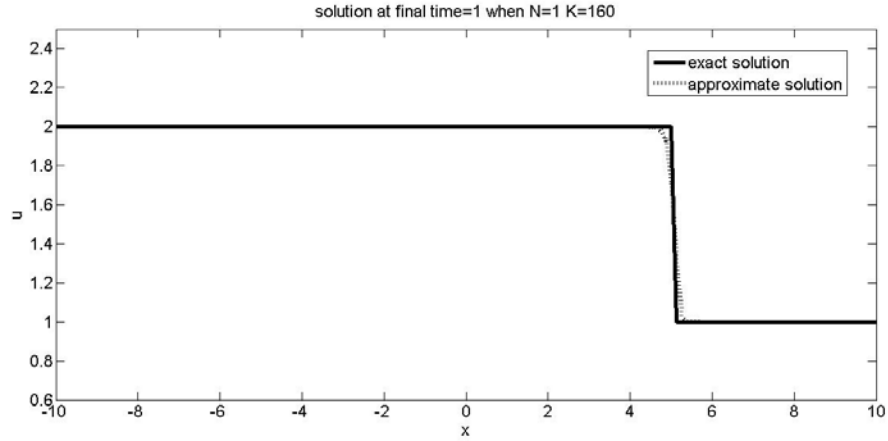


Figure 5.3: The comparison between the exact solution and the approximate solution at the final time $T = 1$ when $N = 1$ and $K = 160$.

The RMS errors for various number of polynomial degrees and the number of cells are shown in Table 5.2. For fixed degree of polynomial basis in the calculations, it is found that numerical error decreases as the number of cells increases but it is in the same order of 10^{-2} which is not agree with the results in Theorem 3.1 and Theorem 3.2 because the solution is not smooth enough in this case.

The numerical observations from this case are different from the case of smooth initial data since when we try to increase the order of polynomial basis, it cannot improve accuracy of the numerical solution. Thus, for high gradient profile, the accuracy of numerical solution can be improved only by increasing resolutions or the number of cells. Increment of polynomial basis order does not provide high accuracy solution for discontinuous case. But increasing the number of cells to get high accuracy solution is directly resulting to large computation time. This issue motivates us to apply the adaptive mesh criteria to increase resolution especially near the shock area that adaptive polynomial method should not improve accuracy in this case.

N/K	20	40	80	160
1	0.1017	0.0844	0.0691	0.0562
2	0.1040	0.0766	0.0559	0.0398
3	0.1045	0.0805	0.0600	0.0436

Table 5.2: The RMS errors for RKDG method using $N = 1, 2,$ and 3 and $K = 20, 40, 80,$ and 160 .

5.1.2 Adaptive polynomial RKDG method for advection equation

In the case of smooth initial condition, we found that using high order of polynomial basis provides more accurate numerical results than using lower order basis. From this finding, we then apply the adaptive polynomial RKDG method for solving the advection equation with initially smooth condition to save the computational time.

We consider the pure advection equation with the same initially smooth conditions (5.4) and (5.5) which has the exact solution (5.6). We then show some numerical results by varying the values of θ_1 and θ_2 , and consider different initial degree of polynomial, maximum degree of polynomial, and the number of cells.

We denote P^N as the numerical solutions obtained from the RKDG method without adaptive criteria with polynomial degree N , and P^l/P^h as the numerical results obtained from the adaptive polynomial RKDG with initial degree l and the maximum degree h .

Case1 Error indicator

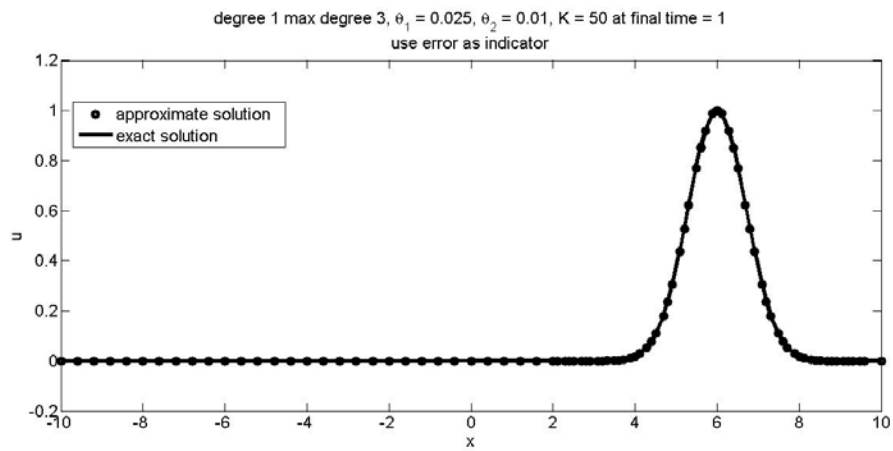


Figure 5.4: The comparison of the exact solution and the numerical solution at the final time $T = 1$ using error indicator.

We show the accuracy of numerical solutions by the adaptive polynomial RKDG method using error indicator in Figure 5.4, where the initial degree is 1 and the maximum degree is 3. Here, θ_1 and θ_2 are 0.025 and 0.01 respectively. We can see that the numerical solution (circle) is in good agreement with the exact solution (solid line) including around the peak area.

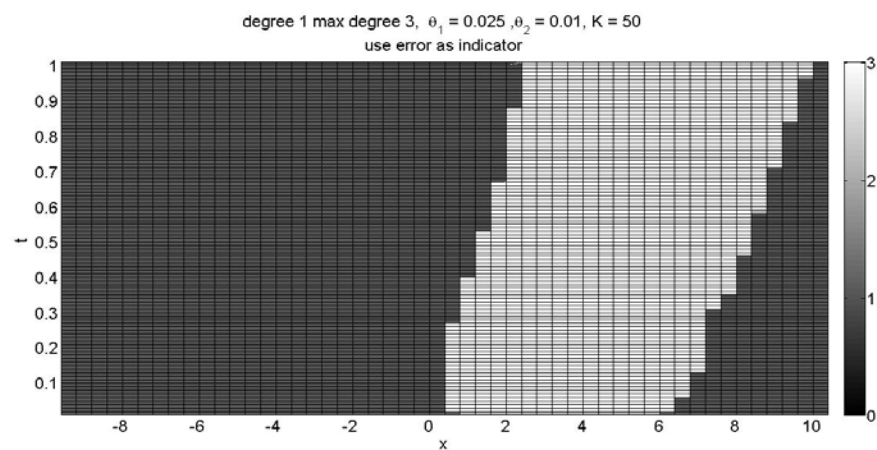


Figure 5.5: The $x - t$ plot shows adaptive polynomial method from degree 1 to degree 3.

The degrees of polynomial for each cell in the time domain is shown in Figure 5.5. For each time, the error indicator can detect the troubled cells which are moving with the same speed as of the solution profile. The troubled cells are in the high gradient areas. The color bar shows the values of degrees of polynomial. The polynomial degree increases from one to three for the troubled cells. Also, we can see that the troubled cells are released to usual cells as the solution moves to the right, polynomial degree decreases from three to one. The polynomial degrees in each cell of Figure 5.4 is shown by Figure 5.5 at $T = 1$. Cells for $2 \leq x \leq 10$ have been adapted by increasing degrees of polynomial.

	$(\theta_1, \theta_2) = (0.1, 0.05)$	$(\theta_1, \theta_2) = (0.025, 0.01)$	$(\theta_1, \theta_2) = (0.01, 0)$
P^1	1.6468e-003	1.6468e-003	1.6468e-003
P^2	7.6041e-005	7.6041e-005	7.6041e-005
P^3	2.5861e-006	2.5861e-006	2.5861e-006
P^1/P^2	1.3456e-004	8.9834e-005	8.3948e-005
P^1/P^3	2.8599e-004	2.8096e-005	9.8543e-006
P^2/P^3	1.6238e-005	2.8713e-006	2.7624e-006

Table 5.3: The RMS errors using error indicator with $K = 100$ cells and for some values of θ_1 and θ_2 .

From Table 5.3, when the values of θ_1 and θ_2 are fixed and without adaptive polynomial criteria, the results obtained by the higher degrees are more accurate than results calculated using the lower degrees of polynomial as expected to the results from theory. The RMS error of P^2 is comparable with P^1/P^2 . They are in the same order, however the P^2 method gives more slightly accurate results. Likewise, the results from the P^3 and the P^2/P^3 methods are comparable. The P^3 method provides slightly better results. The RMS errors of P^1/P^3 are less than P^1 but are in the same order of P^3 when using small values of θ_1 and θ_2 . These results show that the computational cells have been adapted from degree one to degree three until the numerical solution has the RMS error in the same order as the maximum degree of polynomial applied. Numerical results by other adaptive

degrees of polynomial can be concluded similarly.

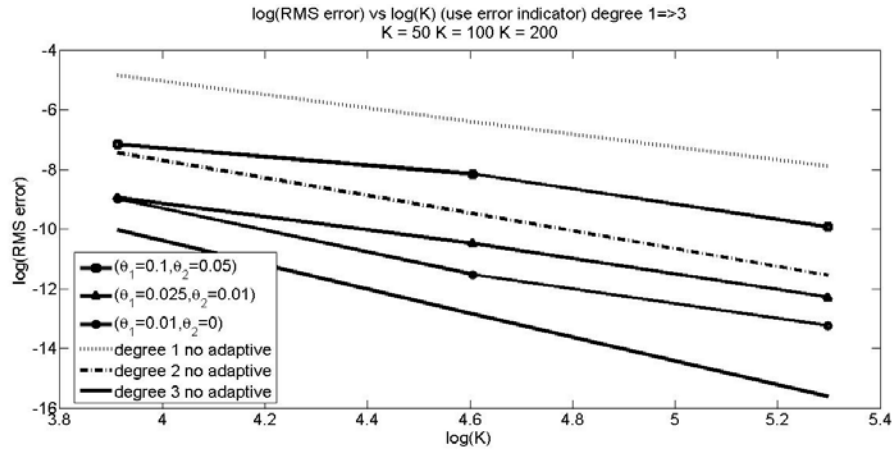


Figure 5.6: The relationship between $\log(\text{RMS error})$ and $\log(K)$ for various values of θ_1 and θ_2 when $\text{mindeg}=1$ and $\text{maxdeg} = 3$, error indicator is applied. Number of cells are $K = 50, 100$, and 200 .

In Figure 5.6, in case of without adaptive polynomial criteria, the RMS errors decrease as the number of cells increase. The rate of convergence is approximately of $O(N + 1)$ where N is the degree of polynomial. When we apply the adaptive method, the RMS error decrease as the values of θ_1 and θ_2 decrease because many cells have been detected as trouble cells when θ_1 and θ_2 decrease.

Case2 Gradient indicator

The numerical results obtained by the adaptive polynomial with gradient indicator are shown in this section. The objective is to show the efficiency of this indicator and compare to that results by the error indicator.

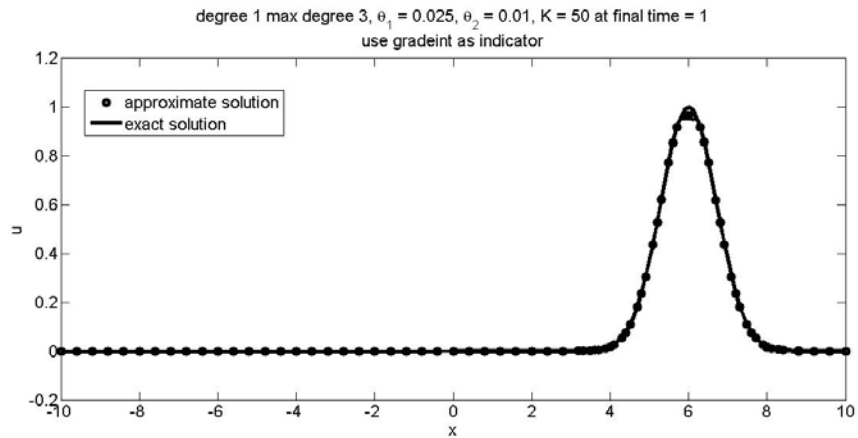


Figure 5.7: The comparison of the exact solution with the numerical solution at the final time $T = 1$, using gradient indicator.

The accuracy of numerical results obtained by the adaptive polynomial with the gradient indicator method is shown in Figure 5.7. The profile is in good agreement with the exact solution except around the peak area. However, if we want to improve the solution accuracy in this area, we have to set the values of θ_1 and θ_2 to be sufficiently small in order to detect more troubled cells near the peak because the gradient is quite small in this area.

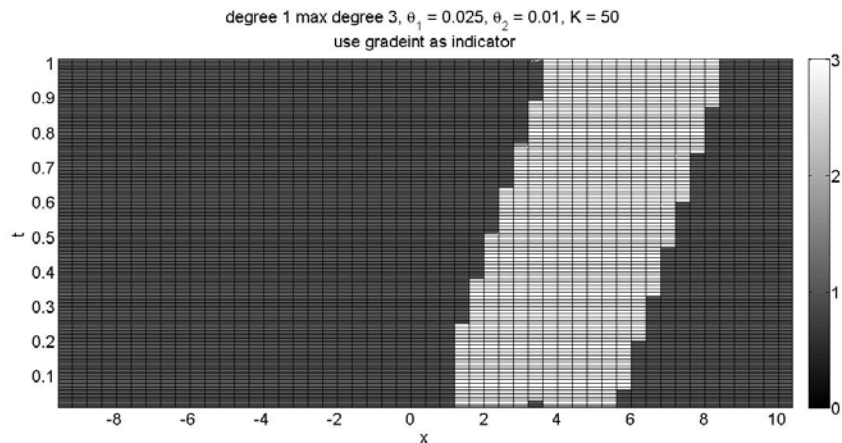


Figure 5.8: The $x - t$ plot shows adaptive polynomial cells from degree 1 to degree 3.

The degree of polynomial for each cell in the time domain is shown Figure 5.8.

It is shown that the gradient indicator can detect trouble-cell zone similar to the case of the error indicator except some cells around the peak area.

	$(\theta_1, \theta_2) = (0.1, 0.05)$	$(\theta_1, \theta_2) = (0.025, 0.01)$	$(\theta_1, \theta_2) = (0.01, 0)$
P^1	1.6468e-003	1.6468e-003	1.6468e-003
P^2	7.6041e-005	7.6041e-005	7.6041e-005
P^3	2.5861e-006	2.5861e-006	2.5861e-006
P^1/P^2	3.1666e-004	1.1455e-004	9.0263e-005
P^1/P^3	3.5018e-004	8.1399e-005	3.4526e-005
P^2/P^3	1.0345e-005	4.2764e-006	3.1197e-006

Table 5.4: The RMS errors when using the gradient indicator with $K = 100$ cells for some values of θ_1 and θ_2 .

The RMS errors using the adaptive polynomial with gradient indicator for various values of θ_1 and θ_2 are shown in Table 5.4. The conclusions are similar to those of using error indicator. That is, the adaptive polynomial method provides more accurate results than the method without using adaptive criteria.

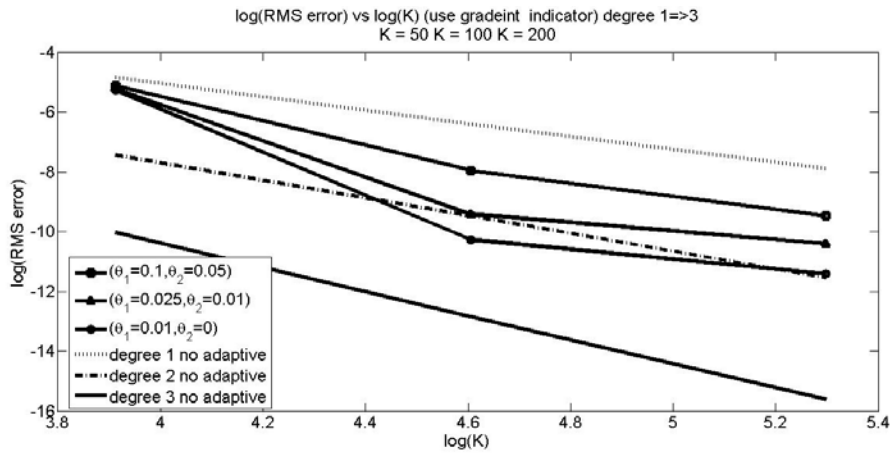


Figure 5.9: The relationship between $\log(\text{RMS error})$ and $\log(K)$ for various values of θ_1 and θ_2 when $\text{mindeg} = 1$ and $\text{maxdeg} = 3$, gradient indicator is applied. Number of cells are $K = 50, 100,$ and 200 .

The relationship between $\log(\text{RMS error})$ and $\log(K)$ is shown in Figure 5.9.

The RMS errors decrease as the number of cells increase. The rate of convergence of numerical solution in the case of without using adaptive method is of $O(N + 1)$ as expected. When we apply the adaptive polynomial method, the RMS error decreases as the values of θ_1 and θ_2 decrease because many cells have been detected as troubled cells when θ_1 and θ_2 are sufficiently small.

5.1.3 Adaptive mesh RKDG method for advection equation

For discontinuous initial condition as shown in section 5.1, the numerical accuracy is not effected by increasing order of polynomial. But accuracy can be improved by increasing the number of cells. Hence, adaptive mesh refinement is suitable for this type of solution.

We consider the pure advection equation with initially discontinuous conditions (5.7) and (5.8). The exact solution is in (5.9).

Some numerical results are shown by using adaptive mesh method when fixing the degree of polynomial. We have varied four different values of $maxlev$ from 1 to 4 in the adaptive mesh algorithm. Thus, $maxlev = 4$ corresponds to the smallest divided cell from the primary cell which $maxlev = 0$ is set at the initial computation.

Case1 Error indicator

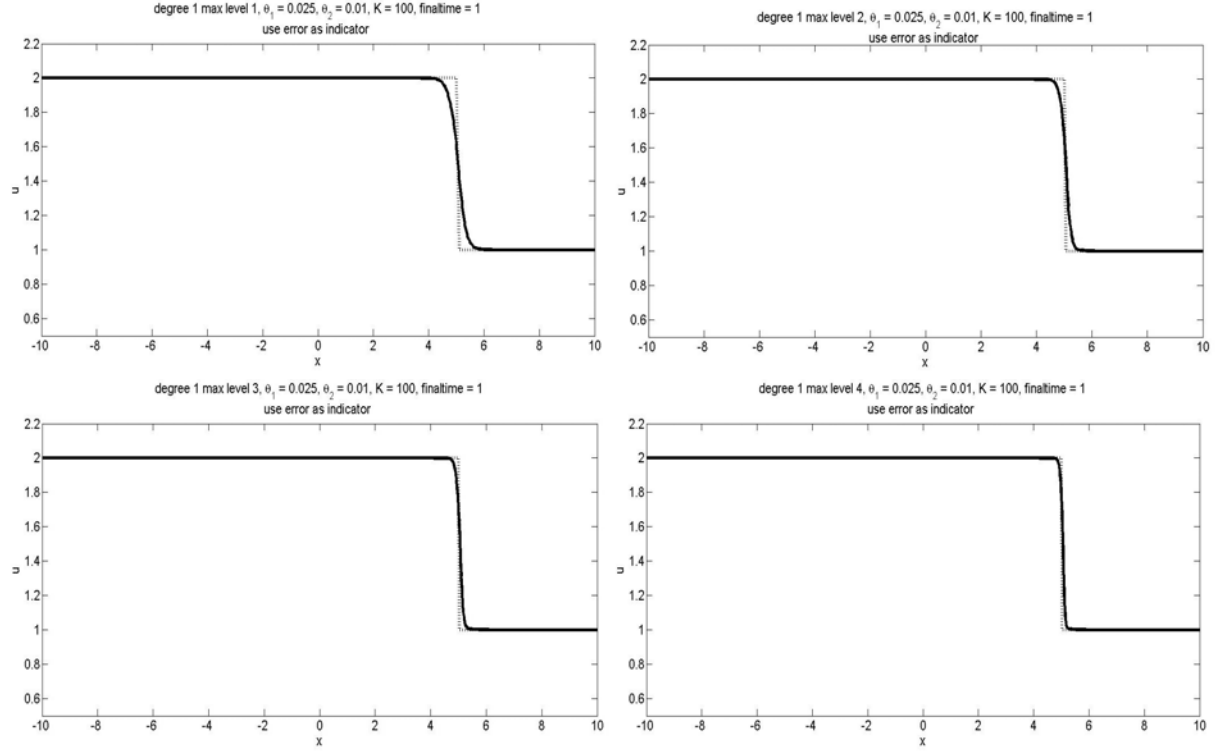


Figure 5.10: The comparisons between the exact solution (dot line) and the numerical solution (solid line) at the final time $T = 1$, using error indicator in the adaptive mesh method for four cases of $maxlev$: $maxlev = 1$ (top-left), $maxlev = 2$ (top-right), $maxlev = 3$ (bottom left), and $maxlev = 4$ (bottom-right).

In Figure 5.10, We have set θ_1 and θ_2 as $(\theta_1, \theta_2) = (0.025, 0.01)$. It is shown at $T = 1$ that the sharp-front can be captured accurately when setting $maxlev = 4$ because more cells have been detected as troubled cells and these cell are divided in to smaller sub-cells. The smallest mesh spacing occurs at $maxlev = 4$.

When we use polynomial degree 1 as a basis function, the results of various values of θ_1 and θ_2 are shown in Table 5.5. The notation P_{maxlev}^N refers to the results of using polynomial degree N as a basis with $maxlev$ in the adaptive mesh method. We can see that for fixing degree of polynomial, the RMS error decreases as the $maxlev$ increases. The results in Table 5.5 are plotted in Figure 5.11.

	$(\theta_1, \theta_2) = (0.1, 0.05)$	$(\theta_1, \theta_2) = (0.025, 0.01)$	$(\theta_1, \theta_2) = (0.01, 0)$
P^1	0.0647	0.0647	0.0647
P_1^1	0.0524	0.0524	0.0524
P_2^1	0.0435	0.0441	0.0442
P_3^1	0.0381	0.0393	0.0395
P_4^1	0.0362	0.0378	0.0381

Table 5.5: The RMS error when using error indicator with $K=100$, $N=1$ for some values of θ_1 and θ_2 .

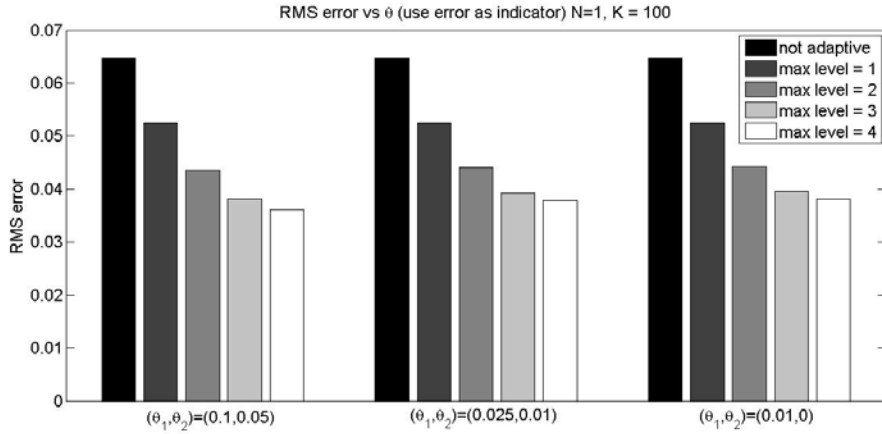


Figure 5.11: The relationship between RMS error and (θ_1, θ_2) when using $N = 1$ as basis function. Error indicator is applied where $K = 100$.

It can be seen from Figure 5.11 that the most accurate results can be obtained using $maxlev = 4$. The RMS error decreases as $maxlev$ increases. The errors are not directly effected by the values of θ_1 and θ_2 because the troubled cells appear only around the shock area and the number of troubled cells are not different for each pair of θ_1 and θ_2 .

The results by the adaptive mesh method with error indicator when fixing degree of polynomial $N = 2$ are shown in Table 5.6 and Figure 5.12. The conclusions are similar to those the case of using polynomial degree $N = 1$.

	$(\theta_1, \theta_2) = (0.1, 0.05)$	$(\theta_1, \theta_2) = (0.025, 0.01)$	$(\theta_1, \theta_2) = (0.01, 0)$
P^2	0.0492	0.0492	0.0492
P_1^2	0.0399	0.0384	0.0404
P_2^2	0.0294	0.0294	0.0310
P_3^2	0.0231	0.0227	0.0233
P_4^2	0.0191	0.0204	0.0204

Table 5.6: The RMS error when using error indicator with $K=100$, $N=2$ for some values of θ_1 and θ_2 .

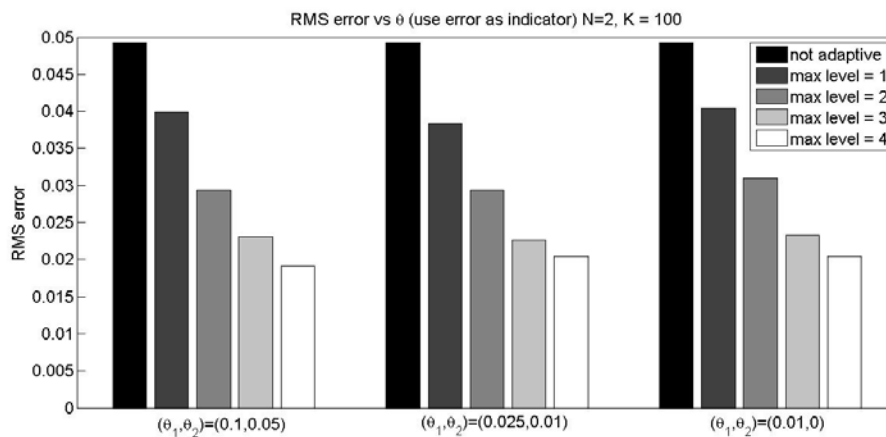


Figure 5.12: The relationship between RMS error and (θ_1, θ_2) when using $N = 2$ as basis function. Error indicator is applied where $K = 100$.

Case2 Gradient indicator

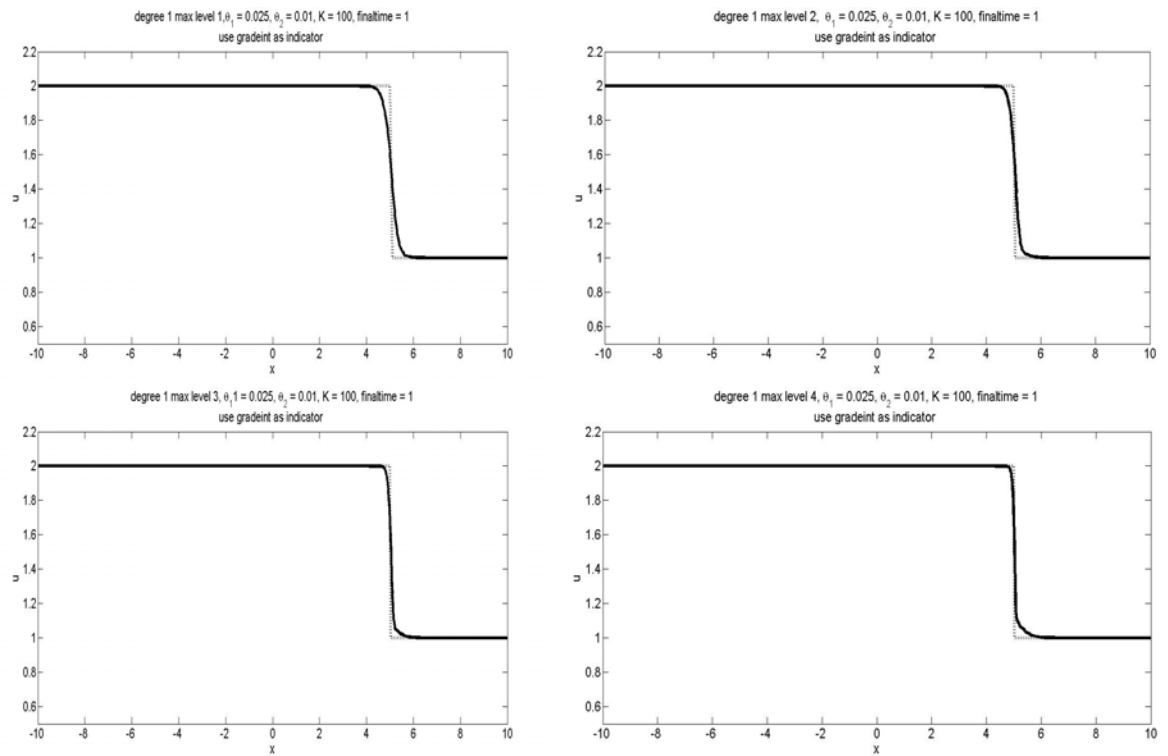


Figure 5.13: The comparisons between the exact solution (dot line) and the numerical solution (solid line) at the final time $T = 1$, using gradient indicator in the adaptive mesh method for four cases of maxlev : $\text{maxlev} = 1$ (top-left), $\text{maxlev} = 2$ (top-right), $\text{maxlev} = 3$ (bottom left), and $\text{maxlev} = 4$ (bottom-right).

It can be seen from Figure 5.13 that the results and the area of troubled cells from gradient indicators are similar to the error indicators. The sharp front is well captured as maxlev increased.

	$(\theta_1, \theta_2) = (0.1, 0.05)$	$(\theta_1, \theta_2) = (0.025, 0.01)$	$(\theta_1, \theta_2) = (0.01, 0)$
P^1	0.0647	0.0647	0.0647
P_1^1	0.0523	0.0524	0.0524
P_2^1	0.0426	0.0435	0.0439
P_3^1	0.0375	0.0368	0.0385
P_4^1	0.0658	0.0300	0.0353

Table 5.7: The RMS error when using gradient indicator with $K=100$, $N=1$ for some values of θ_1 and θ_2 .

It can be seen from Table 5.7 that the most accurate result can be obtained by using $maxlev=4$, and the RMS errors are not directly effected by the values of θ_1 and θ_2 . However, for case of $(\theta_1, \theta_2) = (0.1, 0.05)$, these values are relatively large so that the trouble cells cannot be detected correctly like in the case of $(\theta_1, \theta_2) = (0.025, 0.01)$. The $(x - t)$ plot showing the adaptive mesh area is presented in Figure 5.14. The troubled cell zone for the case of $(\theta_1, \theta_2) = (0.1, 0.05)$ is smaller when comparing with the case of $(\theta_1, \theta_2) = (0.025, 0.01)$.

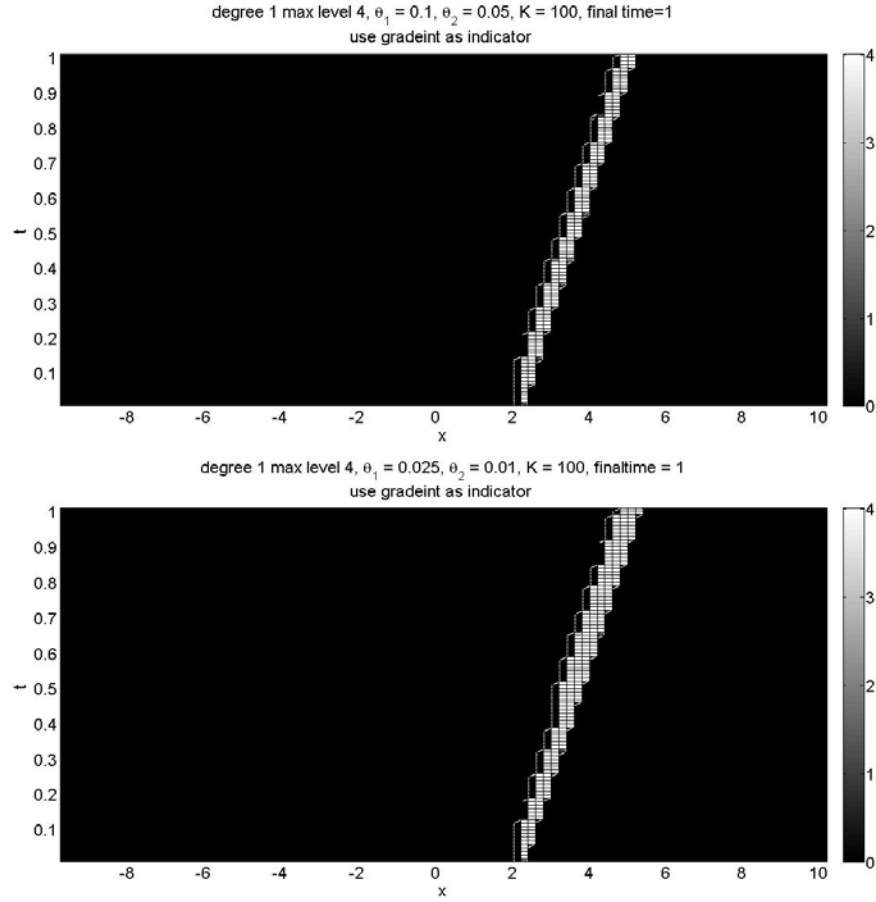


Figure 5.14: The adaptive area for $N = 1$, $K = 100$, $(\theta_1, \theta_2) = (0.1, 0.05)$ (top) and $(\theta_1, \theta_2) = (0.025, 0.01)$ (bottom) with gradient indicator.

	$(\theta_1, \theta_2) = (0.1, 0.05)$	$(\theta_1, \theta_2) = (0.025, 0.01)$	$(\theta_1, \theta_2) = (0.01, 0)$
P^2	0.0492	0.0492	0.0492
P_1^2	0.0415	0.0419	0.0411
P_2^2	0.0351	0.0319	0.0307
P_3^2	0.0388	0.0258	0.0231
P_4^2	0.0549	0.0245	0.0199

Table 5.8: The RMS error when using gradient indicator with $K = 100$ cells, polynomial degree $N = 2$ for some values of θ_1 and θ_2 .

The results by the adaptive mesh method with gradient indicator when fixing

polynomial degree 2 are shown in Table 5.8. The conclusions are similar to those the case of using degree 1. We can obtain the highest accurate results if we use sufficient small values of θ_1 , θ_2 , and $maxlev = 4$.

5.2 Shallow Water Equations

In this section, we show some numerical results using the RKDG method and the adaptive mesh RKDG methods for solving the shallow water equations. For adaptive cases, we used two indicators to detect the troubled cells in the computational domain as applied before in the advection equation. In this thesis, we restrict our attentions to the shallow water equations with no source term, i.e., $S(U) = 0$.

Let the initial condition be

$$h(x, 0) = \begin{cases} h_L, & \text{if } x < 0, \\ h_R, & \text{if } x > 0. \end{cases} \quad (5.10)$$

For wet bed problem, $h_R > 0$ and for dry bed problem, $h_R = 0$. The fluid is assumed initially at rest or equivalently the initial velocity is zero.

When we set $h_L = 1$ and $h_R = 0$, the exact solution for the dry bed case can be expressed as

$$h(x, t) = \begin{cases} 1, & \text{if } x \leq t, \\ \frac{1}{9} \left(2 - \frac{x}{t}\right)^2, & \text{if } -t \leq x \leq 2t, \\ 0, & \text{if } 2t \leq x. \end{cases} \quad (5.11)$$

If we set $h_L = 1$, $h_R = a$ where $0 < a < 1$, the exact solution for the wet bed case is,

$$h(x, t) = \begin{cases} 1, & \text{if } x \leq -1, \\ \frac{1}{9} \left(2 - \frac{x}{t}\right)^2, & \text{if } -t \leq x \leq (u_2 - h_2)t, \\ h_2, & \text{if } (u_2 - h_2)t \leq x \leq Vt, \\ a, & \text{if } Vt \leq x. \end{cases} \quad (5.12)$$

where h_2 , u_2 and V can be found numerically by the Newton's method when the value of a is specified.

a	h_2	u_2	V
0.9	0.94933	0.05132	0.98763
0.8	0.89715	0.10564	0.97555
0.7	0.84309	0.16360	0.96394
0.6	0.78661	0.22618	0.95340

Table 5.9: Some values of h_2 , u_2 and V when a is given.

In this thesis, we choose $a = 0.6$ for the wet bed case. More detail derivations of these exact solution can be found in [12] and [14].

5.2.1 RKDG method without adaptive mesh criteria for shallow water equation

Wet bed case

First, consider the wet bed problem with initial condition

$$h(x, t) = \begin{cases} 1, & \text{if } x < 0, \\ 0.6, & \text{if } x > 0. \end{cases} \quad (5.13)$$

The initial velocity is zero.

The solution accuracy by the RKDG method for the wet bed case is shown in Figure 5.15. The approximate solution is in good agreement with the exact solution in the smooth region but smearing near the shock and the rarefaction area.

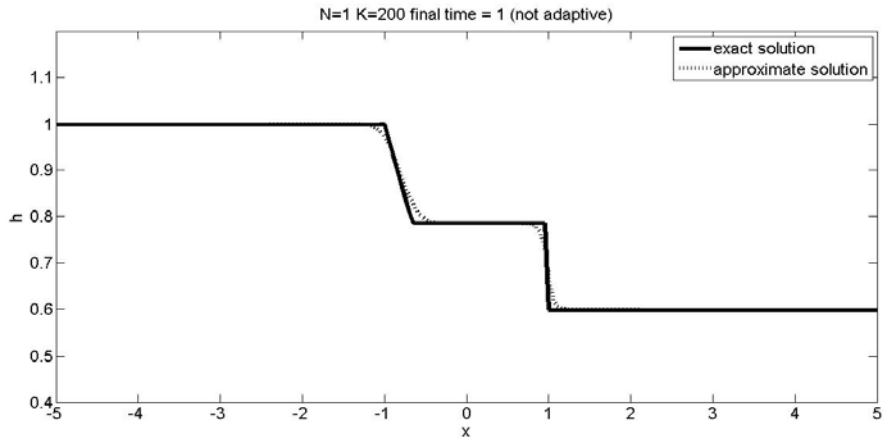


Figure 5.15: The comparison between the exact solution and the numerical solution at final time $T = 1$ using $N = 1$ and $K = 200$ for the wet bed case.

Some numerical results for polynomial degrees $N = 1$ and $N = 2$, with $K = 50, 100$, and 200 are shown in Table 5.10.

N	$K = 50$	$K = 100$	$K = 200$
1	0.0230	0.0145	0.0088
2	0.0184	0.0137	0.0091

Table 5.10: The RMS errors using $N = 1$ and $N = 2$ with $K = 50, 100$, and 200 for the wet bed case.

It can be seen from table 5.10 that the RMS errors decrease as K increase. However, increasing the degree of polynomial basis cannot improve solution accuracy. It is also confirmed that we have to increase numerical resolution instead of increasing degree of polynomial when we are dealing with moving shock.

Dry bed case

For the dry bed problem, we consider the initial condition given by

$$h(x, t) = \begin{cases} 1 & \text{if } x \leq 0, \\ 0 & \text{if } x > 0. \end{cases} \quad (5.14)$$

The initial velocity is zero.

The free surface profiles for the dry bed case is shown in Figure 5.16. The numerical solution is in good agreement with the exact solution including the rarefaction area, $-1 \leq x \leq 2$.

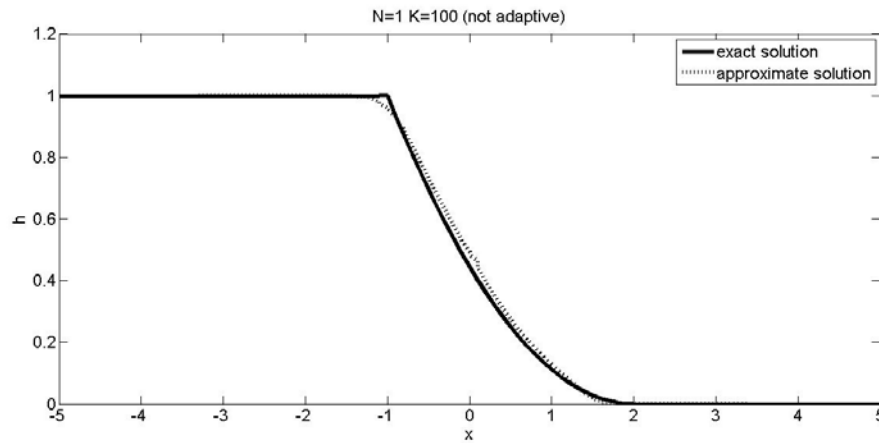


Figure 5.16: The comparison between the exact solution and the numerical solution at the final time $T = 1$ using $N = 1$ and $K = 100$ for wet bed case.

Some numerical results when using polynomial degrees $N = 1$ and $N = 2$, with the number of cell $K = 50, 100$, and 200 are shown in Table 5.11.

N	$K = 25$	$K = 50$	$K = 100$
1	0.0289	0.0288	0.0154
2	0.0489	0.0208	0.0115

Table 5.11: The RMS error using $N = 1$ and $N = 2$ with $K = 25, 50$, and 100 for the dry bed case.

The numerical results are similar to the case of wet bed case. It can be seen from Table 5.11 that the RMS errors decrease as K increase. However, increasing the degree of polynomial basis cannot improve solution accuracy. It is also confirmed that we have to increase numerical resolution instead of increasing degree of polynomial.

5.2.2 Adaptive mesh RKDG method for the shallow water equation

We consider the shallow water equations in two cases, wet bed and dry bed problems. Since the initial condition of both wet bed and dry bed are discontinuous, we can see from Table 5.10, Table 5.11 and the previous results that the results obtained from higher degree of polynomial are not necessary accurate than using lower degree of polynomial. However the accuracy of the numerical solutions can be improved by increasing the number of cells. Hence, this suggest us to employ the adaptive mesh criteria for the case of initially discontinuous condition.

Some numerical results are shown below by using the adaptive mesh method when degree of polynomial is fixed. We have varied $maxlev$ from 1 to 2 in the adaptive mesh algorithm. Thus, $maxlev = 2$ corresponds to the smallest divided cell from the primary cell which $maxlev = 0$ is set at the initial computation.

Wet bed case

We consider the wet bed case with initial condition (5.13) which is the same condition previously performed by the RKDG method.

Case1 Error indicator

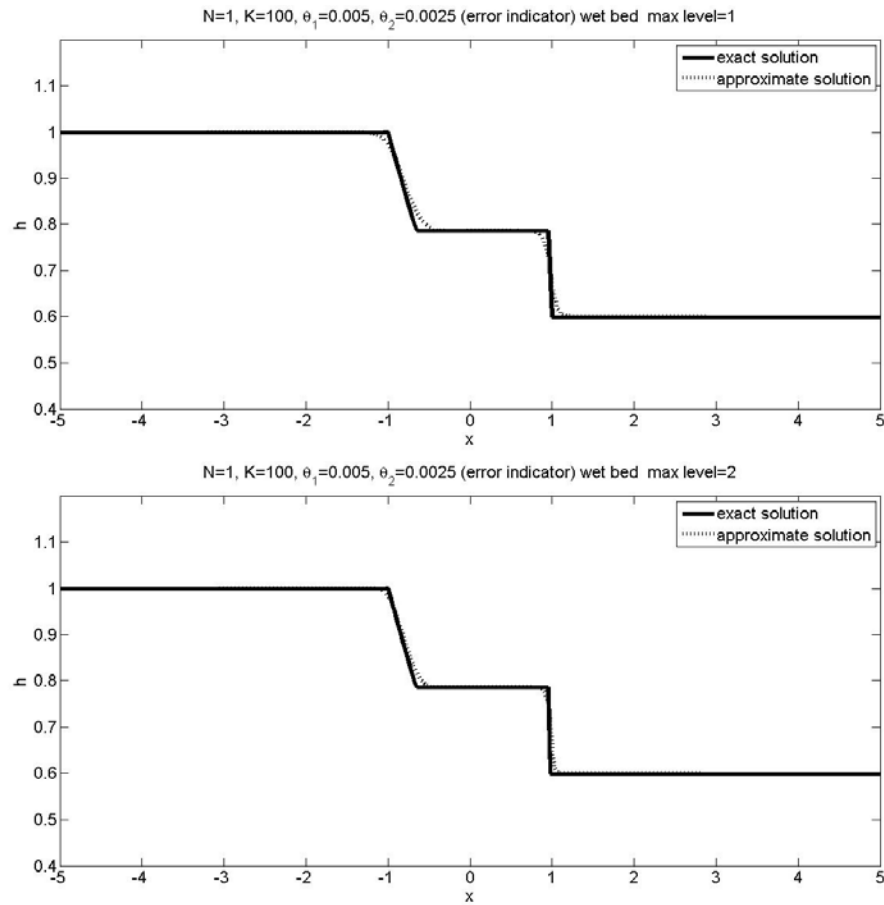


Figure 5.17: The comparisons between the exact solution (solid line) and the approximate solution (dot line) for the wet bed at the final time $T = 1$, using error indicator in the adaptive mesh method for two cases of $maxlev$: $maxlev = 1$ (top) and $maxlev = 2$ (bottom).

In Figure 5.17, we set $N = 1$, $K = 100$, and $(\theta_1, \theta_2) = (0.005, 0.0025)$. It is shown at $T = 1$ that the sharp front and rarefaction can be captured accurately when setting $maxlev = 2$ because many cells have been detected as troubled cells and divided to be smaller sub-cells in the high gradient zone. The smallest mesh spacing occurs at $maxlev = 2$.

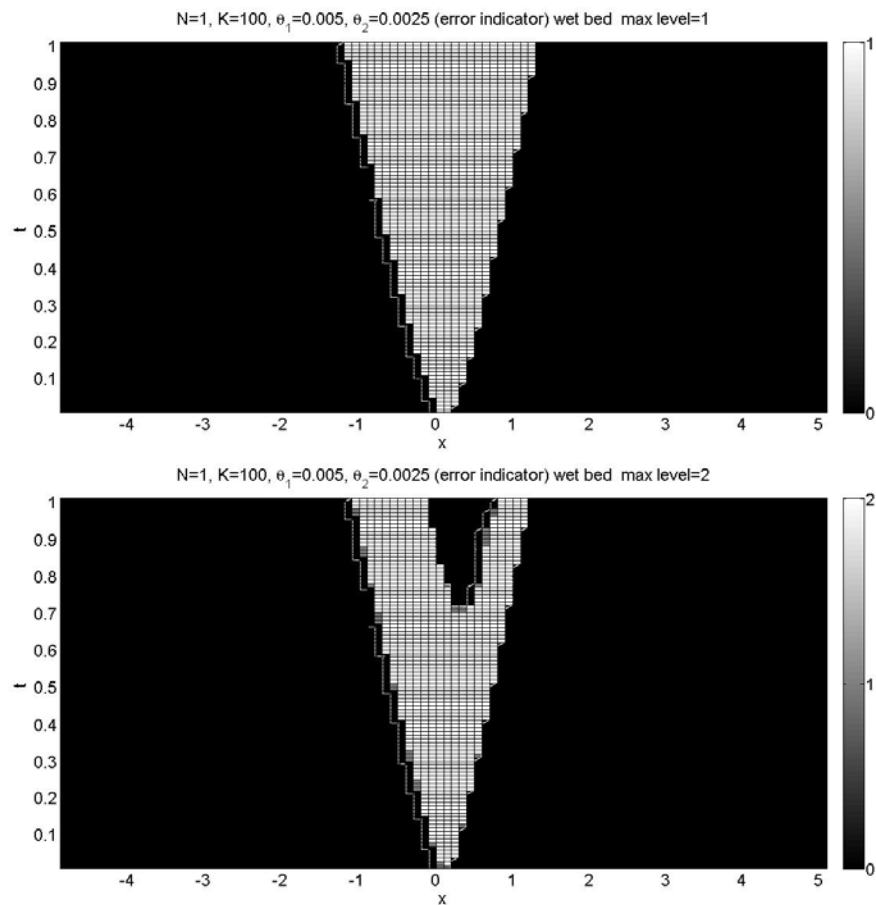


Figure 5.18: The adaptive area for $N = 1$, $K = 100$, $(\theta_1, \theta_2) = (0.005, 0.0025)$ for $maxlev = 1$ (top) and $maxlev = 2$ (bottom) using error indicator.

The level of mesh for each cell in the time domain is shown Figure 5.18. It is shown that, for each time, the error indicator can detect troubled cells which are moving with the solution profile. The troubled cells are lie in the sharp-front and rarefaction areas. The color bar shows the values of mesh level in each time.

When we use polynomial degree 1 or 2 as a basis function, the numerical results for various $maxlev$ comparing with the RKDG method without adaptive mesh criteria are shown in Table 5.12. It can be seen that for a fixed degree of polynomial, the RMS error decreases as the $maxlev$ increases.

$maxlev$	K=50	K=100	K=200	$maxlev$	K=50	K=100	K=200
P^1	0.0230	0.0145	0.0088	P^2	0.0184	0.0137	0.0091
P_1^1	0.0145	0.0088	0.0060	P_1^2	0.0137	0.0089	0.0058
P_2^1	0.0111	0.0075	0.0053	P_2^2	0.0093	0.0060	0.0043

Table 5.12: The RMS error using $N = 1$ and $N = 2$ with $K = 50, 100,$ and 200 and $(\theta_1, \theta_2) = (0.005, 0.0025)$ for the wet bed case, error indicator is applied.

Case2 Gradient indicator

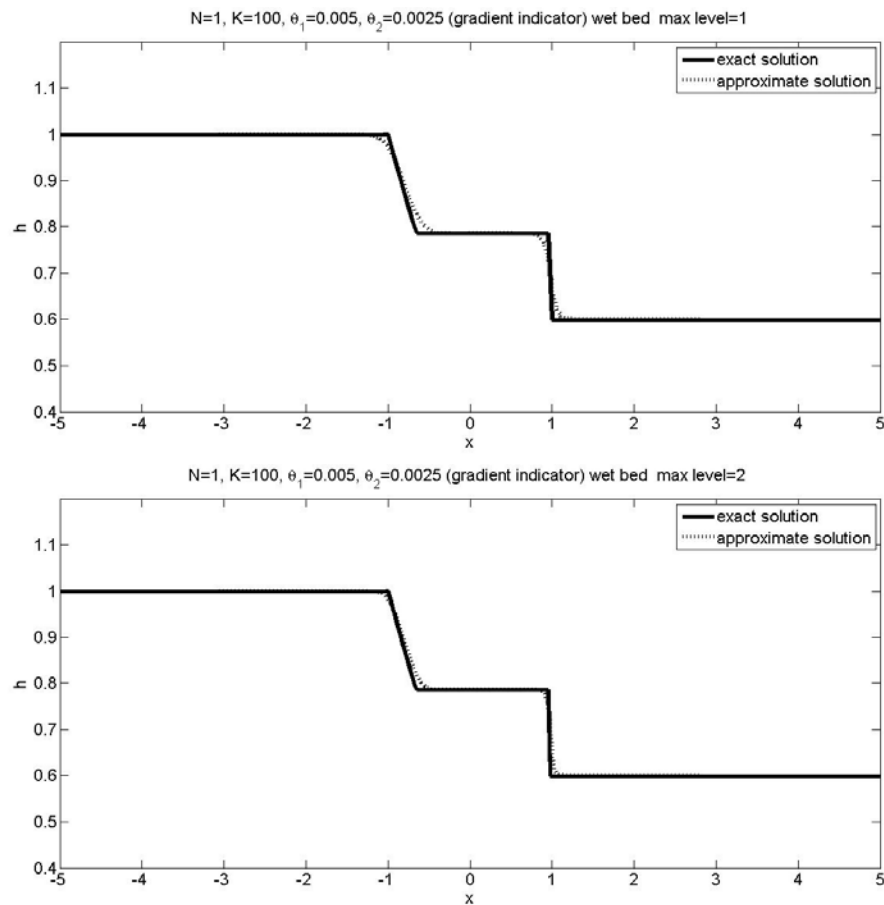


Figure 5.19: The comparisons between the exact solution(solid line) and the numerical solution(dot line) for the wet bed problem at the final time $T = 1$, using the gradient indicator in the adaptive mesh method for two cases of $maxlev$: $maxlev = 1$ (top) and $maxlev = 2$ (bottom).

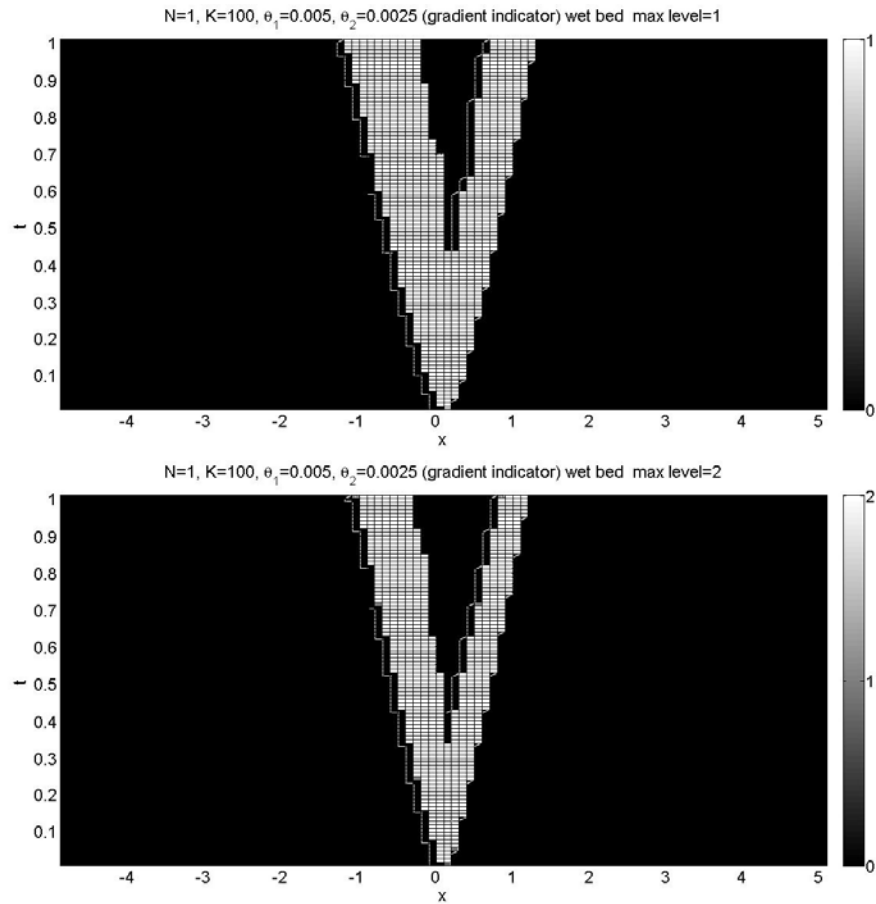


Figure 5.20: The adaptive area for $N = 1$, $K = 100$, and $(\theta_1, \theta_2) = (0.005, 0.0025)$ for $maxlev = 1$ (top) and $maxlev = 2$ (bottom), when the gradient indicator is applied.

It can be seen from Figure 5.19 that the gradient indicator can detect the area of troubled cells, similar to that has been done by the error indicator. The level of mesh for each cell in the time domain is shown in Figure 5.20. The results are similar to those results obtained by the error indicator. The sharp-front and the rarefaction area are well captured when $maxlev$ is increased. When we use polynomial degree 1 and 2 as a basis function, the results of various $maxlev$, comparing with the RKDG method without adaptive mesh criteria are shown in Table 5.13. These numerical results are similar to those the case of using the error indicator, i.e., the RMS errors decrease as the $maxlev$ increase.

max level	K=50	K=100	K=200	max level	K=50	K=100	K=200
P^1	0.0230	0.0145	0.0088	P^2	0.0184	0.0137	0.0091
P_1^1	0.0145	0.0088	0.0060	P_1^2	0.0121	0.0085	0.0074
P_2^1	0.0111	0.0075	0.0053	P_2^2	0.0100	0.0061	0.0043

Table 5.13: The RMS error using $N = 1$ and $N = 2$ with $K = 50, 100,$ and 200 $(\theta_1, \theta_2) = (0.005, 0.0025)$ for the wet bed problem, gradient indicator is applied.

Dry bed case

We consider the dry bed case with initial condition (5.14) which is the same condition previously performed by the RKDG method.

Case1 Error indicator

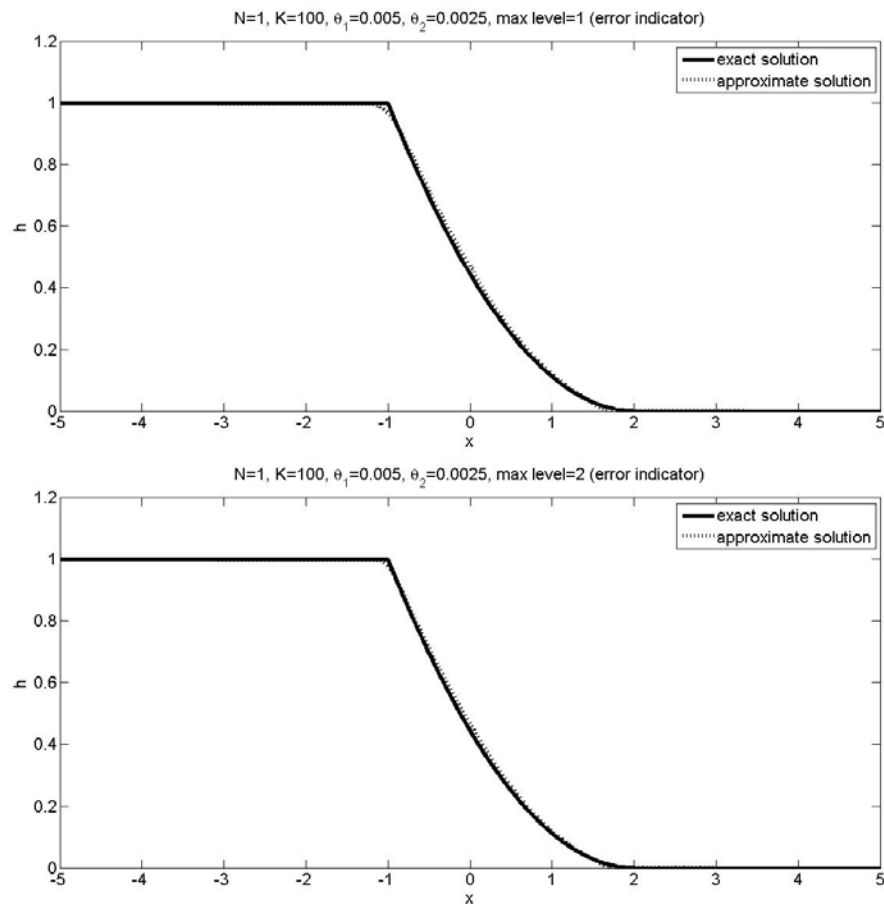


Figure 5.21: The comparisons between the exact solution (solid line) and the approximate solution (dot line) for the dry bed problem at the final time $T = 1$, using error indicator in the adaptive mesh method for two cases of $maxlev$: $maxlev = 1$ (top) and $maxlev = 2$ (bottom).

In Figure 5.21, we set $N = 2$, $K = 50$, and $(\theta_1, \theta_2) = (0.005, 0.0025)$. It is shown at $T = 1$ that the rarefaction can be captured accurately when setting $maxlev = 2$ because many cells have been detected as troubled cells and are refined to smaller sub-cells in the high gradient zone. The smallest mesh spacing occurs at $maxlev = 2$.

The level of mesh for each cell in the time domain is shown Figure 5.22. It is

shown that, at each time, the error indicator can detect troubled cells which are moving with the solution profile. The troubled cells are lie in the rarefaction areas. The color bar shows the values of mesh level in each time.

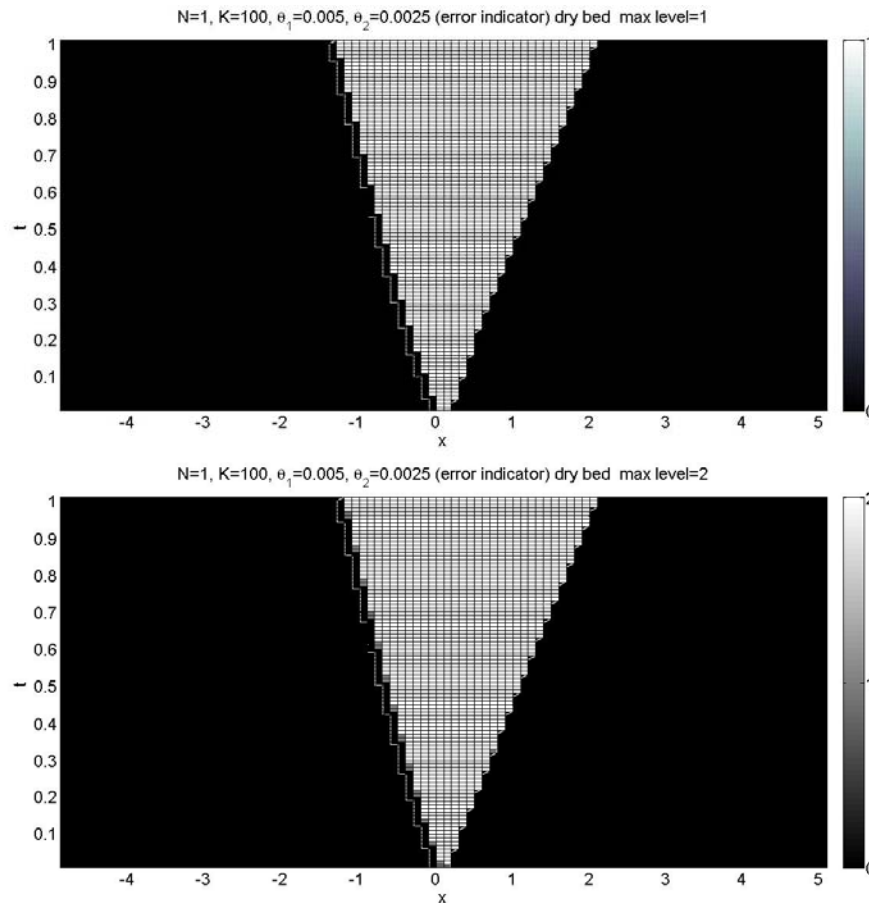


Figure 5.22: The adaptive area for $N = 1$, $K = 100$, and $(\theta_1, \theta_2) = (0.005, 0.0025)$ for $maxlev = 1$ (top) and $maxlev = 2$ (bottom) for error indicator.

When we use polynomial degrees 1 or 2 as a basis function, the numerical results for various $maxlev$, comparing with the RKDG method without adaptive mesh criteria, are shown in Table 5.14. Similar to wet bed case, It can be seen that for a fixed degree of polynomial, the RMS errors decrease as the $maxlev$ increase.

<i>maxlev</i>	K=25	K=50	K=100	<i>maxlev</i>	K=25	K=50	K=100
P^1	0.0289	0.0288	0.0154	P^2	0.0489	0.0208	0.0115
P_1^1	0.0287	0.0154	0.0082	P_1^2	0.0208	0.0111	0.0061
P_2^1	0.0265	0.0139	0.0071	P_2^2	0.0151	0.0082	0.0043

Table 5.14: The RMS error using $N = 1$ and $N = 2$ with $K = 25, 50$, and 100 and $(\theta_1, \theta_2) = (0.005, 0.0025)$ for the dry bed case, error indicator is applied.

Case2 Gradient indicator

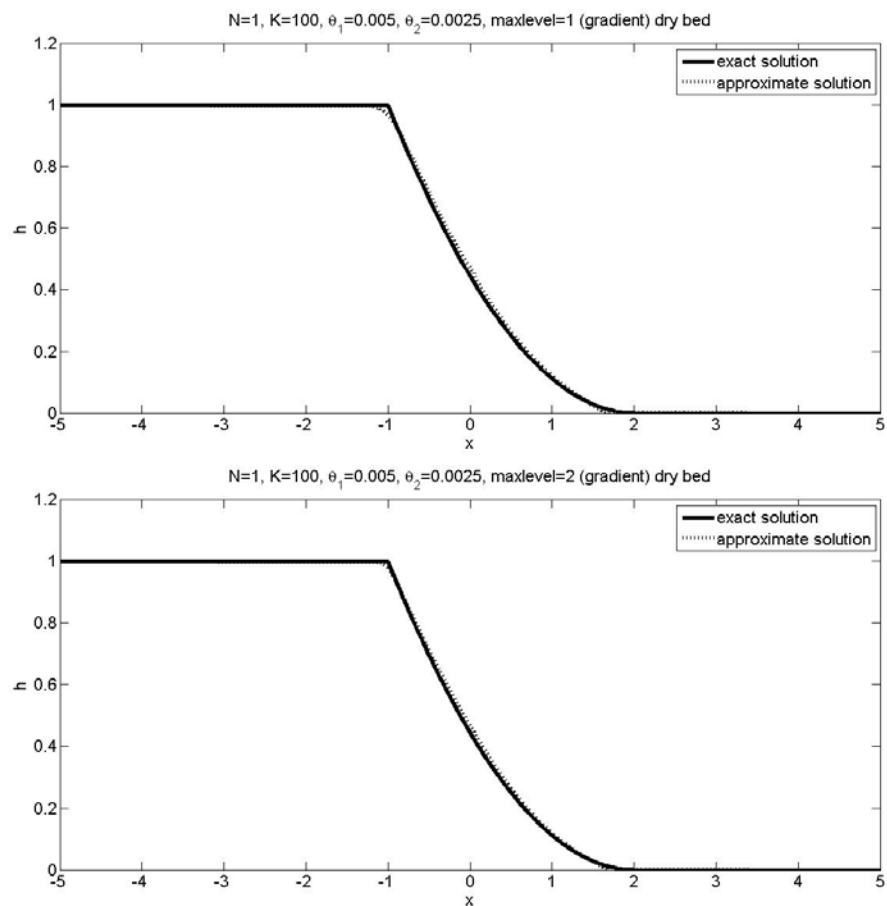


Figure 5.23: The comparisons between the exact solution (solid line) and the numerical solution (dot line) for dry bed problem at the final time $T = 1$, using gradient indicator in the adaptive mesh method for two cases of *maxlev*: *maxlev* = 1 (top) and *maxlev* = 2 (bottom).

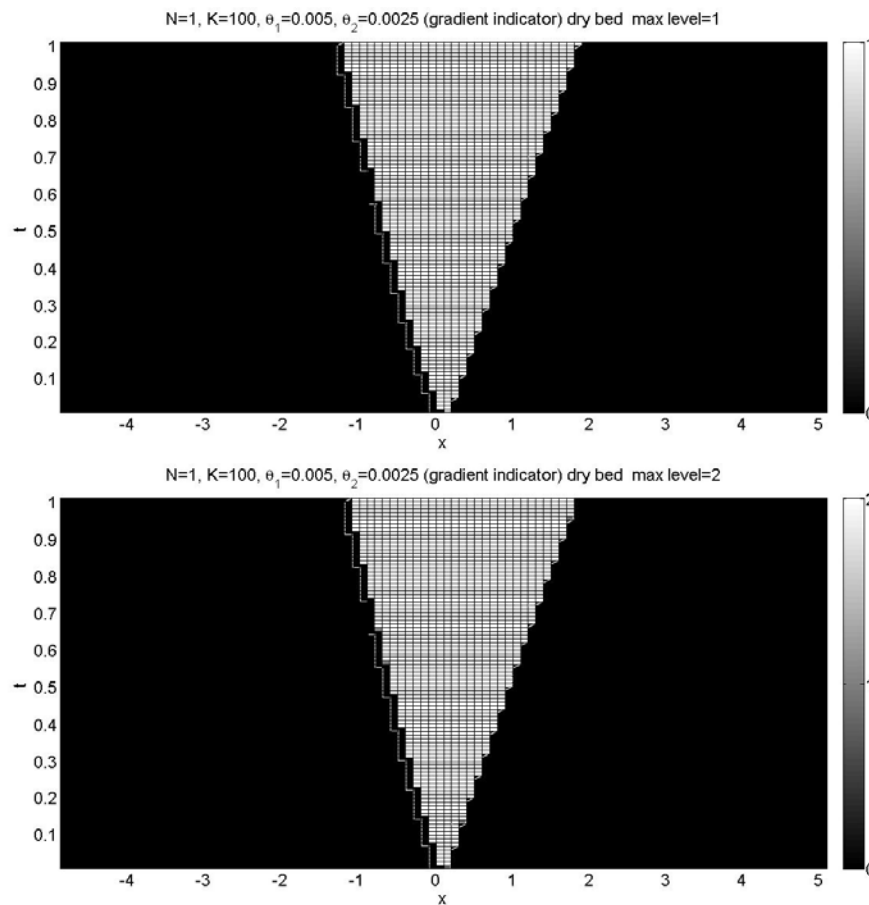


Figure 5.24: The adaptive area for $N = 1$, $K = 100$, and $(\theta_1, \theta_2) = (0.005, 0.0025)$ for $maxlev = 1$ (top) and $maxlev = 2$ (bottom) with the gradient indicator is applied.

It can be seen from Figure 5.23 that the gradient indicator can detect the area of troubled cells similar to that has been done by the error indicator. The level of mesh for each cell in the time domain is shown in Figure 5.24. The results are similar to those results obtained by the error indicator. The rarefaction area are well captured when $maxlev$ is increased. And when we use polynomial degrees 1 and 2 as a basis function, the results of various $maxlev$, comparing with the RKDG method without adaptive mesh criteria are shown in Figure 5.15. These numerical results are similar to those the case of using the error indicator, i.e., the RMS errors decrease as the $maxlev$ increase.

<i>maxlev</i>	K=25	K=50	K=100	<i>maxlev</i>	K=25	K=50	K=100
P^1	0.0289	0.0288	0.0154	P^2	0.0489	0.0208	0.0115
P_1^1	0.0287	0.0154	0.0082	P_1^2	0.0208	0.0111	0.0061
P_2^1	0.0265	0.0139	0.0071	P_2^2	0.0151	0.0082	0.0043

Table 5.15: The RMS error using $N = 1$ and $N = 2$ with $K = 25, 50$, and 100 , $(\theta_1, \theta_2) = (0.005, 0.0025)$ for the dry bed problem, gradient indicator is applied.

CHAPTER VI

CONCLUSIONS

In this thesis, we have presented the adaptive RKDG method for solving the one-dimensional advection equation and the shallow water equations. For the advection equation, we consider both the smooth initial condition and the discontinuous initial condition. For shallow water equations, we consider two problems which are the wet bed and dry bed problems with discontinuous initial condition.

There are two types of adaptive algorithms presented in this thesis, the adaptive polynomial for solving the smooth initial condition and the adaptive mesh for solving the discontinuous initial condition. We also present two types of indicators which are the error and gradient indicators. The indicators are used to detect troubled cells in the computational domain before applying the adaptive criteria. The adaptive polynomial is appropriate for increasing the accuracy of numerical solutions in the case of the smooth solutions. Our presented approach can increase automatically the degree of polynomial basis for troubled cells, and reversely it can decrease automatically the degree of polynomial if that cells are usual. The highest accuracy can be obtained if the maximum degree is used. However, increasing order of polynomial basis cannot improve accuracy for sharp-front solution, the adaptive mesh refinement is needed in this case. Then, we apply only adaptive mesh criteria for solving the shallow water equations. The numerical results by the adaptive mesh method for the advection equation and the shallow water equations are shown. It is found that the solution accuracy increases as the maximum level increases. For these two criteria, the values of θ_1 and θ_2 are depended on desired order of accuracy. Our presented adaptive mesh method are successfully applied to capture some shock interfaces, rarefaction and high gradient areas in our model problems.

REFERENCES

- [1] A. Harten and H. Tal-Ezer. *On a Fourth Order Accurate Implicit Finite Difference Scheme for Hyperbolic conservation Laws.II Five-point Scheme*, Journal of Computational Physics 41 (1981), 329-356.
- [2] B. Cockburn, C.W. Shu, Johnson Claes and E. Tadmor. *Advanced Numerical Approximation of Nonlinear Hyperbolic Equations: Lectures Given at the 2nd Session of the Centro Internazionale Matematico Estivo (C.I.M.E.) held in Cetraro, Italy , June 23-28, 1997*, Springer-Verlag Telos, 1998.
- [3] B. Cockburn and C.W. Shu. *TVB Runge-Kutta Local projection Discontinuous Finite Element Method for conservation Laws II. General Framework*, Mathematics of computation 52 (1989), 411-435.
- [4] B. van Leer. *Toward the ultimate conservation difference scheme ii.*, Comput. Phys. 14 (1974), 361-376.
- [5] B. van Leer. *Toward the ultimate conservation difference scheme v.*, Comput. Phys. 32 (1979),1-136.
- [6] D. Schwanenberg, R. Kiem, and J. Kongeter. *A discontinuous Galerkin method for the shallow-water equations with source terms. Discontinuous Galerkin Methods: Theory, Computations and Applications*, B. Cockburn, G. E. Karniadaki, and C.-W. Chu, Eds., *Lecture Notes in Computational Science and Engineering*, Springer 11 (2000), 419-424
- [7] E. F. Toro. *Riemann Solvers and Numerical Methods for Fluid Dynamics: A Practical Introduction*, Springer, 1999.
- [8] E. F. Toro. *Shock-Capturing Methods for Free-Surface Shallow Flows* , John Willy and sons LTD, 2001.
- [9] E. J. Kubatko, S. Bunya, C. Dawson and J. J. Westerink. *Dynamic p-adaptive Runge-Kutta discontinuous Galerkin methods for the shallow water equations*, Comput. Methods Appl. Mech. Engrg. 198 (2009), 1766-1774.
- [10] G. Manzini. *A second-order TVD implicit-explicit finite volume method for time-dependent convection reaction equations*, Mathematics and Computers in simulation. 79 (2009), 2403-2428.
- [11] Hongqiang Zhu and Jianxian Qiu. *Adaptive Runge-Kutta discontinuous Galerkin methods using different indicators: One-dimensional case*, Journal of Computational Physics. 228 (2009), 6957-6976.

- [12] J. D. Logan. *An introduction to nonlinear partial differential equations*, John Willy and sons LTD, 2008.
- [13] J. S. Hesthaven and T. Warburton. *Nodal Discontinuous Galerkin Methods: Algorithms, Analysis, and Applications*, Springer, 2008.
- [14] Kanoknuch Chamsri. Model and simulation of dam-break problem. Master's thesis Mathematics Chulalongkorn University, 2004.
- [15] P. A. Tassi and C. A. Vionnet. *Discontinuous Galerkin Method for the one dimensional simulation of shallow water flows*, Meca`nica Computational Vol. XXII, Bahi´a Blanca. 22 (2003)
- [16] R. J. Leveque. *Finite Volume Method for Hyperbolic Problem*, Cambridge University Press, 2005.
- [17] R. J. Leveque. *Numerical Methods for Conservation Laws*, Birkhuser Verlag, 1992.
- [18] Z. Xu, J. Xu, and C.-W. Shu. *A high order adaptive finite element method for solving nonlinear hyperbolic conservation laws.*, Technical Report 2010-14, Scientific Computing Group, Brown University, Providence, RI, USA, Apr. (2010)

VITA

Name Thida Pongsanguansin

Date of Birth 16 October 1986

Place of Birth Bangkok, Thailand

Education B.Sc. (Mathematics, First Class Honors),
Kasetsart University, 2009

Scholarship Science Achivement Scholarship Thailand(SAST)

Publication Thida pongsanguansin, Khamron Mekchay and
Montri Maleewong, *Adaptive Discontinuous Galerkin
Method for One-Dimensional Advection Equation. Annual
Pure and Applied Mathematics Conference (2011), 41-56*